

Response to Anonymous Referee #1

The reviewer's comments are in black and our answers are in blue. Snippets of text from the submitted manuscript are in italics while modifications of the manuscript are shown in bold italics. The pages and lines reported here correspond to the submitted manuscript.

General comments: The paper titled ‘Thin ice clouds in the Arctic: Cloud optical depth and particle size retrieved from ground-based thermal infrared radiometry’ presents a new retrieval algorithm to estimate cloud optical depth and separate TIC1 vs TIC2 clouds based on the effective particle diameter. The paper contributes to the remote sensing field, is within the scope of AMT, and builds upon existing work that is well-referenced but some additional details are required. Results and conclusions are presented clearly and overall the paper is well-structured. Prior to publication I have several comments which need to be addressed:

We are grateful to this reviewer for the helpful comments. We provide below a point-by-point reply to his comments.

Specific comments:

-P.1-2: the introduction is well-structured but fairly brief. Please consider highlighting the relevance and importance of these observations to other communities (satellite, modelers, etc.) by describing additional applications (e.g., reference the satellite cloud climatology project Klein and Jakob, 1999; Webb et al., 2001).

Also, there have been previous studies using similar or even the very same instrumentation (FIRR, AERI) to measure the radiative effect of thin ice clouds. Describing these studies demonstrate the novelty of this paper’s retrieval algorithm. See for instance Libois et al., 2016 (AMT), Blanchet et al., 2011 (SPIE), Mariani et al., 2012 (AMT), and related studies therein.

We have added more explanations about the relevance of ice clouds study in the introduction.

*P1 L17: Predictions of future climate change and its regional and global impacts require that a better understanding of the radiative transfer interactions between clouds, water vapor and precipitation be incorporated into appropriate models. **Recent CMIP5 model intercomparisons (the Coupled Model Intercomparison Project as described in Jiang et al., 2012) indicate large variability in ice cloud parameters (for example ice water content) amongst high-latitude models. Shortcomings in ice cloud parametrization (Baran, 2012) impact their representation of radiative effects as well as water cycles and leads to uncertainties in quantifying cloud feedbacks in the context of climate change (Waliser et al., 2009). High-altitude thin ice clouds consisting of pure ice crystals, which cover between 20 to 40% of the Earth (Wylie and Menzel, 1999), can, for example, have opposing effects on the radiative properties of the Earth.***

*P2L6: **The advent of active sensors onboard satellites (for example CALIPSO/CloudSat) has enabled the application of considerably more resources for polar region ice cloud studies. This permits the evaluation of climate models (Jiang et al, 2012) and satellite cloud climatologies (Sassen et al., 2008). Long-term ground-based observations which are also essential for the validation of models and satellite climatology are, however, limited in their Arctic coverage (Heymsfield, 2017).***

*P 2 L 21: **A proposed satellite-based instrument whose goal will be the characterization of thin ice clouds in the Arctic using far and thermal infrared channels (Blanchet et al., 2011) was recently tested during an airborne campaign in the High Arctic (Libois et al., 2016).***

-P. 2 l. 1-2 and l. 22-24: these statements require references.

P. 2 l. 1-2: *The macrophysical and microphysical properties of thin ice clouds determine which process dominates and hence determine the net forcing of thin ice clouds on the climate system (Stephens, 2005).*

P. 2 l. 22-24: *In this paper, we examine how multi-band thermal measurements of zenith sky radiance can be used to retrieve what are, as indicated in the early remote sensing literature (see Nakajima and King, 1990 for example), the most critical extensive and intensive parameters influencing the radiative effects of ice clouds: cloud optical depth (COD) and effective particle diameter (D_{eff}).*

-P. 3 l. 1-5 these two statements require references.

P3 L1: *Water vapor and clouds are a significant climate modeling challenge since they represent major radiative forcing influences, while being the least understood components of the climate system (Waliser et al., 2009; Jiang et al., 2012).*

P3. L3: *Much of the recent research has been focused on aerosol-cloud interaction processes involving aerosols acting as ice and water cloud nuclei and their subsequent affect on cloud microphysics, precipitation and radiation (see for example, Feingold and McComiskey (2016) on recent ARM campaigns, Winker et al. (2010) and Illingworth et al. (2015) respectively, on the cloud remote sensing mandate of the A-Train and EarthCARE satellite missions and Jouan et al. (2013) as part of the NETCARE project).*

-P. 3 l. 11: Table 1 only lists the instruments used in this study. There are many more instruments operating at Eureka. Please clarify this.

This is true. We have changed the Table 1 caption. *List of the Eureka (PEARL) instruments employed in our analysis.*

-P. 5 l. 5: is there a reference for the CIMEL? An instrument paper is needed for the reader to understand the technical capabilities of the instrument.

A very similar instrument (we used a newer version with 2 additional channels) was fully detailed in Legrand et al. (2000), in terms of performances and error analysis. The companion paper (Brogniez et al., 2003) focused on its behavior in field campaigns and showed radiometric measurement accuracy of about 0.1 K. We have added those references in the manuscript. P5L5 :(see Legrand et al. (2000) and Brogniez et al. (2003) for descriptions of a similar instrument).

-P. 5 l. 6: why are the 10.2-10.9 and 11.8-13.2 channels not centered at the midpoint, but the other channels are? Please also clarify whether the exact same spectral ranges were used for the integrated P-AERI spectra.

By centered, we meant the peak wavelength of the spectral filter response. This was clarified in the manuscript. P.5 L.6: ... and filter response peak values ~~are centered~~ at 8.4, 8.7, 9.2, 10.7, 11.3 and 12.7 μm . As shown in the figure below, the peaks are not always located in the middle of the channel.

The integration over the P-AERI spectra was weighted using the spectral filter response given by the manufacturer (see figure below). This was clarified in the text:

P.5 L.6: *In actual fact however, we had to simulate the response of this radiometer by convolving the*

spectral transmittance of each filter with the spectra of the Eureka Polar AERI (P-AERI) instrument (provided by Von Walden at the U. of Idaho and NOAA).

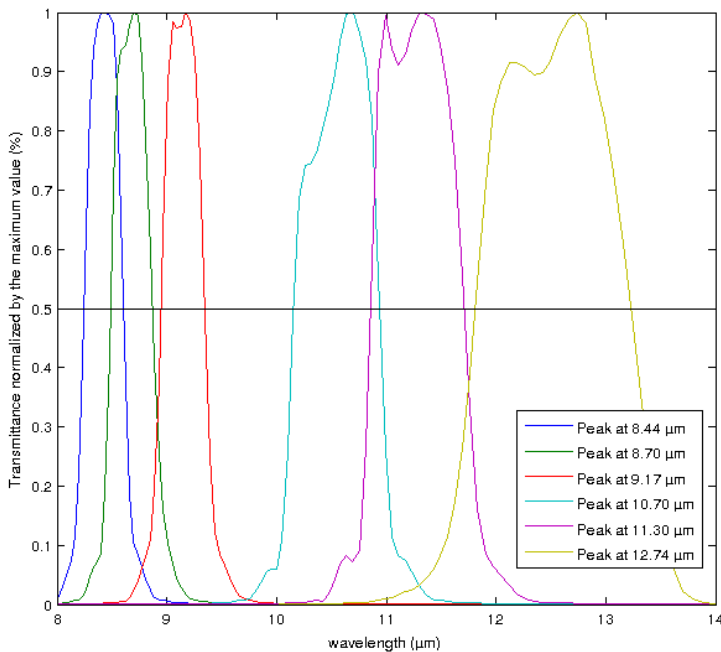


Figure 1: Transmittance of the 6 channels, normalized by their maximum value

-P. 5 l. 9-10: what are the implications of using P-AERI spectra to simulate CIMEL spectra? The impact of different spectral resolution, brightness temperature accuracy, instrument noise, and sampling time should be discussed. For instance, FIRR vs. AERI brightness temperature observations have statistically significant differences, possibly due to thermal affects. Is it possible to include results (if any) that indicate the level of agreement between the CIMEL and an AERI?

We agree that a comparison side-by-side of both instruments (P-AERI and CE-312) would be beneficial to better assess the performances of the radiometer. Unfortunately during field campaigns, the CE-312 wasn't ready for deployment and a slightly different instrument (CE-332), with only 3 bands, was used. The comparison with the 8.7 μm band (Figure 2 below) showed relatively good correlative agreement ($R^2=0.97$) except in the presence of low brightness temperatures (clear sky). The correlative statistics were similar for the 2 other bands (10.8 μm and 12.6 μm), resp. 0.98 and 0.99.

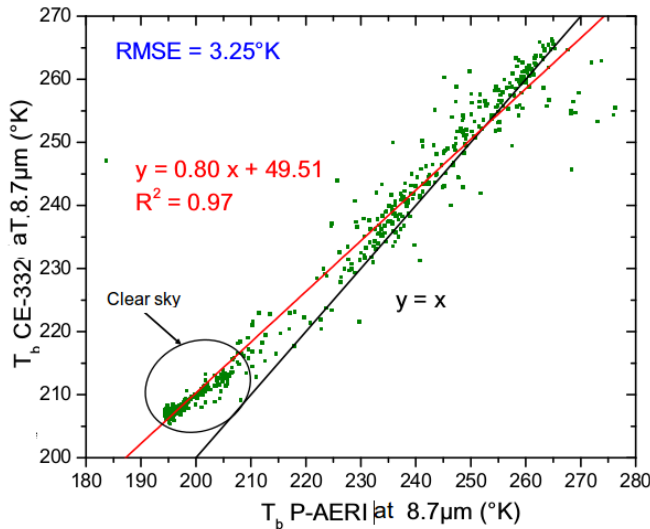


Figure 2: Brightness temperature comparison between integrated P-AERI spectra and the CE-332 8.7 μm channel during the field campaign in September 2007.

The P-AERI, which includes a highly accurate radiometric calibration system that employs 2 blackbody references, is expected to have a higher absolute accuracy (as an indicator of absolute differences relative to the P-AERI, we would note that the rms error relative to the “ $y = x$ ” line on Figure 2 is 9.04 K for all the points and 5.23 K if the “Clear sky” points are not included). The noise equivalent temperature difference (NETD) is less than 30 mK, which can be compared with the value of 50 mK (at 20 °C) for the CE-312 instrument. In spite of the more moderate performance of the CE-332, we would remind the reviewer that the retrieval method incorporates the CE-312 measurement error. It is for this latter reason and the fact that we did not have a full, prototype, 6-band instrument in the field that we decided to not include a comparison of the CE-332 with the P-AERI directly in the text of the article.

-P. 7 l. 9-11: the reference case listed in Table 2 has different cloud base height and thickness values than what is listed in the ‘average’ row, but in the paper it is stated that the reference case was the set of mean parameters. Please clarify.

For the reference case, the cloud base height and thickness values were rounded to the nearest step of the MODTRAN vertical profiles for convenience. We added the following sentence to the legend to explain this: *For the reference case, the cloud base height and thickness values were, for the sake of convenience, rounded to the nearest incremental step of the MODTRAN vertical layer profiles.*

-P. 7: the reference case was for $D_{\text{eff}} = 50$ microns, which is a TIC2 cloud. Please comment on results for a TIC 1 cloud with $D_{\text{eff}} < 30$ microns.

We used a reference value that is common for ice clouds (Sourdeval et al., 2013). If we take a reference D_{eff} value of 15 μm , the sensitivity analysis is relatively similar with moderate differences of $< \sim 1$ K (compare Figure 3 below with Figure 4 in the paper). We added the following sentence to the discussion of Figure 4 (P. 8 L9); *We note that there was little sensitivity to the choice of a 50 μm effective diameter for the reference case: changing this typical TIC2 value to a value more representative of TIC1 particles produced differences of less than 1 K in Figure 4.*

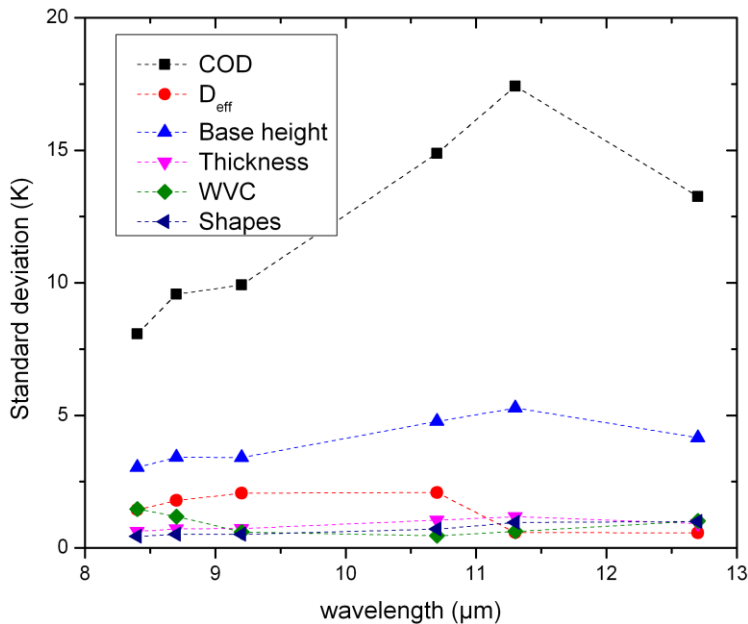


Figure 3: Sensitivity of T_b as a function of the six key radiative transfer parameters, when the reference D_{eff} is set as $15 \mu\text{m}$.

-P. 7: this analysis is heavily dependent on MODTRAN'S ability to accurately simulate these cloud properties. Please comment on MODTRAN's reliability in this regard.

We used MODTRAN4 in this article since the 1 cm^{-1} resolution was adequate for our needs. Its multiple scattering capabilities are as accurate as the user requires: we employed this capability, with sensitivity tests, to ensure accurate calculations in the case of the thicker TICs. MODTRAN4 is flexible in the way it allows the user to configure the thermodynamical state of the atmosphere and the optical properties of complex scattering / absorbing constituents such as clouds. Thus, for example, it allowed us to incorporate the ice cloud properties recently parameterized by Baum et al., (2014) and to replace the standard MODTRAN vertical profiles by Eureka-specific radiosonde profiles of temperature and humidity. The layering capabilities allowed us to include cloud bottom and top height from our lidar profiles and to test the sensitivity of the radiative transfer computations to layer resolution.

-P. 8 l. 20: WVC in the Arctic has a large influence on thermal IR measurements depending on the spectral region (e.g., large influence at 20 microns) and season. Please clarify this.

We reinforced the Figure 4 evidence for weak WVC influence with the following modification of the text describing Figure 4. *P.8 L.20: Water vapor content (WVC) in the atmosphere, which remains relatively low during the polar winter at Eureka, has a weak absorption influence on the in the Arctic, can also slightly influence thermal IR-radiance measurements via band absorption acquired in the CE-312 band.*

-P. 9-10: the discussion of errors requires extensive elaboration, particularly in order to defend the statement on p. 9 l. 2-4. For instance, the use of radiosonde data introduces several issues which need to be addressed, including: 1) dry bias, 2) impact of using soundings during cloud cover vs. clear sky on the retrieval, 3) interpolation of the +/- 12 hour radiosonde profile. Errors associated with the OEM retrieval, such as the S_a , S_e , and error covariance matrices, should be described (perhaps in the appendix) to provide a sense of the magnitude of these errors. The a priori and its covariance matrix must be carefully selected due to their large impact on the retrieval's outcome – more detail is needed

here.

1) The Vaisala radiosondes are known to be subject to dry bias which tends to underestimate the relative humidity by 2-8% (Wang et al., 2013), especially in dry conditions, which could be problematic in an arctic environment. This bias is less severe during nighttime (Turner et al., 2003) and by extension during the Arctic Winter. Some authors (Treffeisen et al., 2007; Rowe et al., 2008) have studied the bias in polar regions and have shown the bias could be up to – 10 % in the worst conditions. However, the 6 channels of the radiometer are far less sensitive to the WVC than to COD, as one can see in Figure 4, and are in an atmospheric window of water vapor. We agree that this could be more problematic for bands in the far infrared.

P10 L6: *Radiosonde humidity sensors are known to be subject to dry bias especially in dry conditions and could yield relative humidity underestimates of 10 % (Rowe et al., 2008). The 6 channels are however far less sensitive to the WVC than to COD (see Figure 4) and therefore the bias is expected to be lower in cloudy conditions.*

2) and 3) To avoid the issue of interpolating radiosondes over extensively long periods of time, the cases were selected as close as possible to radiosonde launch times. Indeed, more than 40 % of the 150 cases occurred at a maximum of 3 hours before or after radiosonde profiles. In the case of temperature, the absolute value of the temporal variations between 2 radiosondes, averaged between 2 and 8 km, during the 3 polar winters, is about 1.72 °C, which means 0.14 °C/hour. The following sentences were added in the text: P10 L6: *To avoid the issue of interpolating radiosondes over extensively long periods of time, the cases were selected as close as possible to radiosonde launch times.*

We agree that a careful definition of covariance matrix and errors is needed in the optimal estimation method (OEM). We have added more details about the covariance matrix in the appendix A.

P 20 L13: *In our case, the reference case of Table 2 was used to define the a priori vector and its covariance matrix. ... The measurement errors depend on the accuracy of the radiometer, which is assumed to be 0.1 K for each band (Brogniez et al., 2003). We presumed the measurement errors are wavelength-independent. ... The components of S_e are close to 0.30 K (between 0.28 and 0.34 K) and of the same order of magnitude as S_y .*

-P. 11 l. 9: please describe why this tolerance value was used.

The value of 10^{-15} 1/m/sr represents approximatively the minimum detectable reflectivity close to the surface, in the MMCR general mode. The minimum detectable reflectivity is an estimate of a minimally significant value that we determined from an analysis of MMCR profiles. The following change was made to the text;... *less than $10^{-15} \text{ m}^{-1} \text{ sr}^{-1}$ (an empirically determined value of minimum detectability) were eliminated from any ...*

-P. 11 l. 29: there are several papers that state the wavelength range of the P-AERI is up to 20 microns. Please clarify this discrepancy.

It is true that the original P-AERI was designed to acquire measurements up to 20 μm (the measurements become noisy after 20 μm). The text in the manuscript was changed to (P11 L29): *Although intervals of P-AERI spectra (wavelength range of 3 - 20 μm)...*

More recent versions of the AERI (for example the Extended-AERI, see Mariani et al., 2012), have more far infrared capabilities.

-P. 14 l. 14: on p. 10 it is states that upper and lower cloud boundaries are obtained where 7 vertical samples (52.5 m) comply with the backscatter requirement. Please clarify this discrepancy (52.5 vs.

200 m).

The vertical resolution of 7.5 m was used in a previous version of this study and is now set as 30 m to smooth the lidar and radar profiles. The value of 200 m is set as the vertical step in the MODTRAN simulations. The value of 120 m (4 x 30 m) is needed to delimit cloud boundaries and therefore used to infer the COD and D_{eff} values from active instruments in the validation part of the manuscript. We didn't set the criteria to be 7 continuous pixels (= 210 m) because in some thin case (see for example in figure 6a, before 18:00), it happens that few pixels, in the vertical profile, don't match the threshold on the lidar signal.

P14 L 14: ... a cloud thickness greater than 200 m (to equal or exceed the MODTRAN vertical layer thickness of 200 m), ...

-P. 15 l. 1-2: please clarify what is meant by “sufficiently accurate.”

By “sufficiently accurate.” we meant that there are very few cases (only 2) retrieved by lidar+radar which have a D_{eff} less than 50 μm . This means that the threshold between TIC1 and TIC2 (30 μm) was chosen in a conservative manner to reduce the crossover between TIC1 and TIC2. We made the following change to the text (P15 L1-2); *the 30 μm crossover criterion from TIC1 to TIC2 is sufficiently well delineated to achieve acceptable classification accuracy*

-It would be interesting to see a comparison between MIXCRA and the Lidar-radar retrieval to provide a sense of how well the two established methodologies compare.

A comparison between MIXCRA and AHSRL/MMCR can be found below. But as this article focuses on the performances of the radiometer, we chose not to include a MIXCRA and AHSRL/MMCR comparison.

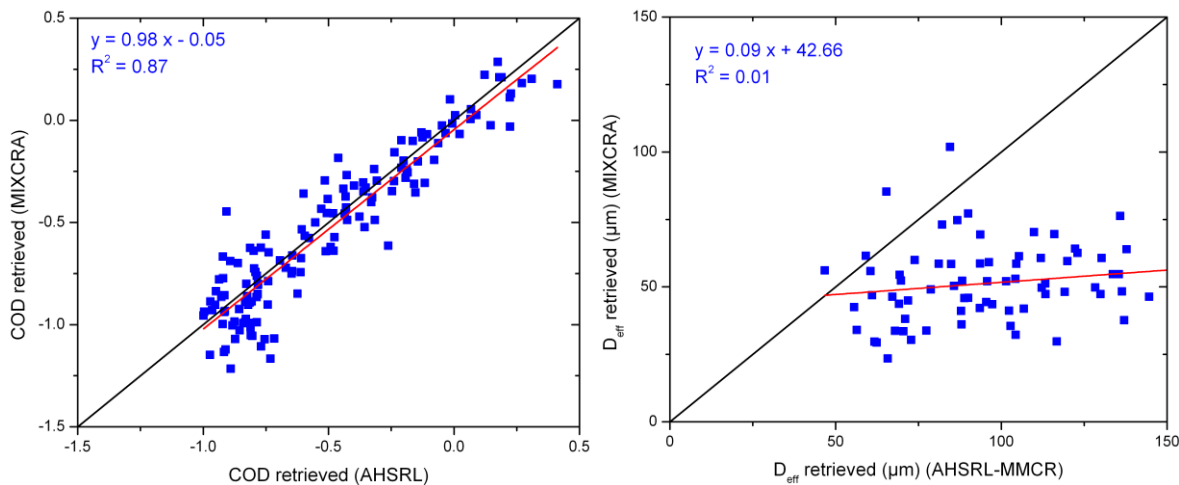


Figure 4: MIXCRA retrieval results compared with lidar derived COD (left) and with the lidar-radar D_{eff} retrieval product (right)

-P. 16 l. 15-on: please clarify whether “the comparison” is between MIXCRA and the AHSRL D_{eff} observations in the Turner and Eloranta paper and state their R-squared result.

P. 16 l. 15: The term “the comparison” was referring to the comparison between our retrievals and MIXCRA (Figure 7d). In actual fact, the paper of Turner and Eloranta (2007) doesn't include comparison of D_{eff} retrievals. To eliminate this source of confusion, we changed the sentence in

question to; “*The comparison of the D_{eff} values from our radiometer retrieval and the MIXCRA retrieval (Figure 7d) shows a somewhat better absolute agreement relative to the comparisons of our radiometer retrieval with the lidar-radar retrieval...*”

-The results discussed regarding Fig. 9 are important and yet left out of the conclusion– consider including them.

We added these sentences at the end of section 6.2 to expand the discussion, rather than in the conclusion, because we thought it would be more relevant: P18: L2. *A long-term analysis would help to support modeling conclusions on the impact of acid-coated ice nuclei on Arctic cloud as reported by Girard et al. (2013). These authors reported a mean downward longwave (negative) radiation anomaly at the surface of -3 -5 W/m², close to Eureka.*

Technical corrections:

-P.2 l. 8-9: the word ‘properties’ is used three times in 12 words.

The sentence was rewritten: *Numerous researchers have exploited the thermal IR behavior of the absorption and scattering efficiencies ~~properties~~ of cloud particles as a means of retrieving ~~those same properties~~—COD and particle effective sizes (e.g., Inoue, 1985).*

-P.2 l.18-19: please consider reordering your examples so that the references are listed in chronological order.

This was done in the manuscript.

-P.2 l. 27-29: the referenced work is not ‘recent,’ as your sources are 22 and 7 years old.

The first reference is important to understand the concept of the dehydration feedback. Since, observations from space (Grenier et al., 2009), airborne campaigns (Jouan et al., 2013) as well as laboratory simulations (Chernoff and Bertram, 2010) and climate model (Girard and Sokhandan, 2014) tends to confirm the impact of acid coating aerosols on cloud microstructure and radiative forcing over the Arctic during the cold season. In any case, we modified the sentence a bit to get rid of “recent”; “*This approach was motivated by **previously published** research that ~~work which shows that indicated~~ such a discrimination would play a key role in characterizing an important aerosol/cloud interaction process in Polar winter, namely precipitative cooling (see, for example, Blanchet and Girard, 1994; Grenier et al., 2009).*”

-P. 3 Eqn. 2: you have explained all variables except D^2 .

P4 L1: *where Q_{ext} is the extinction efficiency (extinction cross section per unit projected-particle-area) (Hansen and Travis, 1974), D is the particle diameter and $a(D)$ is the ice particle number density per unit increment in diameter.*

-P. 4 Fig. 1: no date and observation time is provided in the figure caption. There is also no color bar legend and units.

Corrected.

-P. 5 l. 12: the list of references is not complete. If you are citing examples of studies, then state this using 'e.g.'

Corrected.

-Fig. 2 and Fig. 4: the x-axis label 'lambda' should be changed to reflect what the physical quantity is, i.e., 'Wavelength.' The figure caption should clearly indicate whether this is simulated or observed values.

The term "lambda" was replaced by "wavelength" in the figures.

-Several places in the paper are missing a space. For instance, Table 2 caption, p.7 l.5, caption of Fig. 4.

Corrected.

-The text at the bottom right of Fig. 3 (b) should be moved into the figure caption.

Done.

-Fig. 4: please state the sample size of the simulation both in the figure caption and your discussion.

Done. Figure 4 caption: *Sensitivity of T_b as a function of six key radiative transfer parameters. The standard deviations (in units of K) are obtained by stochastically varying, with a sample size of 1000, the parameters of interest within the limits given in the Table 2. P8L4: ... each parameter individually. These were obtained for 1000 appropriately normalized samples of a random number generator with a normal probability distribution ...*

-P. 11 l. 10: "mean't" should be "meant."

Corrected.

-P. 12 l. 7: avoid nested brackets if possible.

Corrected. *Within the scope of this current study, the cloud-phase determination from MIXCRA is used to ensure the comparison of ice-only cloud properties (i.e. those MIXCRA retrievals that yielded negligible liquid water path, ~~(i.e. $LWP < 0.2 \text{ g.m}^{-2}$)~~, were taken as being pure ice-cloud cases). MIXCRA results are used here as an alternative point of reference for our retrievals.*

-P. 12 l. 12: "and demonstrate that our retrieval produces give physically" – please fix.

We removed the term "produces".

-Fig. 6: titles should be moved next to the color bar (right-hand side). It should be clearly indicated that Fig. 6 (c) is Lidar-Radar retrieval in the figure and/or in the caption.

Done.

-Fig. 6: it is stated that only 8 of the 41 points from (b) passed the screening test. Please identify these points in the figure (perhaps a different color) and explain the distinction in the figure caption.

Done. The figure caption has been modified: *The points upon which a star has been superimposed satisfied the criteria defined at the beginning of section 6.2 and are thus an example of points accepted in the validation part of this article.*

-Fig. 7: the equation ($y=...$) is missing in (b). The RMSE calculations are not shown in (b) and (d). The caption is also quite long – try to shorten and move parts to the discussion.

The equations and RMSE were added in (b) and (d). The caption was shortened.

-P. 20 l. 16: ‘Environment Canada’ is now ‘Environment and Climate Change Canada.’

Corrected.

-P. 22 l. 11-15 and p. 24 l. 10-13: these references are out of order based on publication year.

Done.

References to be added to the article:

Baran AJ. From the single-scattering properties of ice crystals to climate prediction: a way forward. *Atmos Res* 2012;112:45–69.

Baum, B. A., P. Yang, A. J. Heymsfield, A. Bansemer, A. Merrelli, C. Schmitt, and C. Wang, 2014: Ice cloud single-scattering property models with the full phase matrix at wavelengths from 0.2 to 100 μm . *J. Quant. Spectrosc. Radiant. Transfer*, vol. 146, 123-139.

Blanchet, J.-P., Royer, A., Châteauneuf, F., Bouzid, Y., Blanchard, Y., Hamel, J.-F., de Lafontaine, J., Gauthier, P., O’Neill, N. T., Pancrati, O., and Garand, L.: TICFIRE: a far infrared payload to monitor the evolution of thin ice clouds, doi:10.1117/12.898577, <http://dx.doi.org/2010.1117/12.898577>, 2011.

Brogniez, G., C. Pietras, M. Legrand, P. Dubuisson, and M. Haeffelin, 2003: A High-Accuracy Multiwavelength Radiometer for In Situ Measurements in the Thermal Infrared. Part II: Behavior in Field Experiments. *J. Atmos. Oceanic Technol.*, 20, 1023–1033, doi: 10.1175/1520-0426(2003)20<1023:AHMRFI>2.0.CO;2.

Chernoff, D. I., and A. K. Bertram (2010), Effects of sulfate coatings on the ice nucleation properties of a biological ice nucleus and several types of minerals, *J. Geophys. Res.*, 115, D20205,

Feingold, G. and A. McComiskey, 2016: ARM’s Aerosol–Cloud–Precipitation Research (Aerosol Indirect Effects). *Meteorological Monographs*, 57, 22.1–22.15, doi: 10.1175/AMSMONOGRAPHS-D-15-0022.1.

Girard, E., G. Dueymes, P. Du and A.K. Bertram, 2013: Assessment of the Effects of Acid-Coated Ice Nuclei on the Arctic Cloud Microstructure, Atmospheric Dehydration, Radiation and Temperature during Winter. *International Journal of Climatology*. 33, 599-614. DOI: 10.1002/joc.3454

Girard, E. and SokhandanAsl, N. Relative importance of acid coating on ice nuclei in the deposition and contact modes for wintertime Arctic clouds and radiation, *Meteorol Atmos Phys* (2014) 123: 81. doi:10.1007/s00703-013-0298-9

Heymsfield, A., M. Krämer, A. Luebke, P. Brown, D. Cziczo, C. Franklin, P. Lawson, U. Lohmann, G. McFarquhar, Z. Ulanowski, and K. Van Tricht, 2017: Cirrus Clouds. *Meteorological Monographs*, 58, 2.1–2.26, doi: 10.1175/AMSMONOGRAPHS-D-16-0010.1.

Illingworth, A., H. Barker, A. Beljaars, M. Ceccaldi, H. Chepfer, N. Clerbaux, J. Cole, J. Delanoë, C. Domenech, D. Donovan, S. Fukuda, M. Hiraoka, R. Hogan, A. Huenerbein, P. Kollias, T. Kubota, T. Nakajima, T. Nakajima, T. Nishizawa, Y. Ohno, H. Okamoto, R. Oki, K. Sato, M. Satoh, M. Shephard, A. Velázquez-Blázquez, U. Wandinger, T. Wehr, and G. van Zadelhoff, 2015: The EarthCARE Satellite: The Next Step Forward in Global Measurements of Clouds, Aerosols, Precipitation, and Radiation. *Bull. Amer. Meteor. Soc.*, 96, 1311–1332, doi: 10.1175/BAMS-D-12-00227.1.

Jiang, J. H., et al. (2012), Evaluation of cloud and water vapor simulations in CMIP5 climate models using NASA “A-Train” satellite observations, *J. Geophys. Res.*, 117, D14105, doi:10.1029/2011JD017237.

Jouan, C., Pelon, J., Girard, E., Ancellet, G., Blanchet, J. P., and Delanoë, J.: On the relationship between Arctic ice clouds and polluted air masses over the North Slope of Alaska in April 2008, *Atmos. Chem. Phys.*, 14, 1205-1224, doi:10.5194/acp-14-1205-2014, 2014.

Legrand, M., C. Pietras, G. Brogniez, M. Haeffelin, N. Abuhassan, and M. Sicard, 2000: A High-Accuracy Multiwavelength Radiometer for In Situ Measurements in the Thermal Infrared. Part I: Characterization of the Instrument. *J. Atmos. Oceanic Technol.*, 17, 1203–1214, doi: 10.1175/1520-0426(2000)017<1203:AHAMRF>2.0.CO;2.

Libois, Q., Ivanescu, L., Blanchet, J.-P., Schulz, H., Bozem, H., Leaitch, W. R., Burkart, J., Abbatt, J. P. D., Herber, A. B., Aliabadi, A. A., and Girard, É.: Airborne observations of far-infrared upwelling radiance in the Arctic, *Atmos. Chem. Phys.*, 16, 15689-15707, doi:10.5194/acp-16-15689-2016, 2016.

Mariani, Z., Strong, K., Wolff, M., Rowe, P., Walden, V., Fogal, P. F., Duck, T., Lesins, G., Turner, D. S., Cox, C., Eloranta, E., Drummond, J. R., Roy, C., Turner, D. D., Hudak, D., and Lindenmaier, I. A.: Infrared measurements in the Arctic using two Atmospheric Emitted Radiance Interferometers, *Atmos. Meas. Tech.*, 5, 329-344, doi:10.5194/amt-5-329-2012, 2012.

Nakajima, T. and M. King, 1990: Determination of the Optical Thickness and Effective Particle Radius of Clouds from Reflected Solar Radiation Measurements. Part I: Theory. *J. Atmos. Sci.*, 47, 1878–1893, doi: 10.1175/1520-0469(1990)047<1878:DOTOTA>2.0.CO;2.

Rowe, P., L. Miloshevich, D. Turner, and V. Walden, 2008: Dry Bias in Vaisala RS90 Radiosonde Humidity Profiles over Antarctica. *J. Atmos. Oceanic Technol.*, 25, 1529–1541, doi: 10.1175/2008JTECHA1009.1.

Sassen, K., Z. Wang, and D. Liu (2008), Global distribution of cirrus clouds from CloudSat/Cloud-Aerosol Lidar and Infrared Pathfinder Satellite Observations (CALIPSO) measurements, *J. Geophys. Res.*, 113, D00A12, doi:10.1029/2008JD009972

Sourdeval, O., -Labonnote, L. C., Brogniez, G., Jourdan, O., Pelon, J., and Garnier, A.: A variational approach for retrieving ice cloud properties from infrared measurements: application in the context of two IIR validation campaigns, *Atmos. Chem. Phys.*, 13, 8229-8244, doi:10.5194/acp-13-8229-2013, 2013.

Stephens, G., 2005: Cloud Feedbacks in the Climate System: A Critical Review. *J. Climate*, 18, 237–273, doi: 10.1175/JCLI-3243.1.

Treffeisen, R., Krejci, R., Ström, J., Engvall, A. C., Herber, A., and Thomason, L.: Humidity observations in the Arctic troposphere over Ny-Ålesund, Svalbard based on 15 years of radiosonde data, *Atmos. Chem. Phys.*, 7, 2721-2732, doi:10.5194/acp-7-2721-2007, 2007.

Turner, D.D., B.M. Lesht, S.A. Clough, J.C. Liljegren, H.E. Revercomb, and D.C. Tobin, 2003: Dry bias and variability in Vaisala radiosondes: The ARM experience. *J. Atmos. Oceanic Technol.*, 20, 117-132.

Waliser, D., et al. (2009), Cloud ice: A climate model challenge with signs and expectations of progress, *J. Geophys. Res.*, 114, D00A21, doi:10.1029/2008JD010015.

Wang, J., L. Zhang, A. Dai, F. Immler, M. Sommer, and H. Vömel, 2013: Radiation Dry Bias Correction of Vaisala RS92 Humidity Data and Its Impacts on Historical Radiosonde Data. *J. Atmos. Oceanic Technol.*, 30, 197–214, doi: 10.1175/JTECH-D-12-00113.1.

Winker, D., J. Pelon, J. Coakley, S. Ackerman, R. Charlson, P. Colarco, P. Flamant, Q. Fu, R. Hoff, C. Kittaka, T. Kubar, H. Le Treut, M. McCormick, G. Mégie, L. Poole, K. Powell, C. Trepte, M. Vaughan, and B. Wielicki, 2010: The CALIPSO Mission: A Global 3D View of Aerosols and Clouds. *Bull. Amer. Meteor. Soc.*, 91, 1211–1229, doi: 10.1175/2010BAMS3009.1.

Response to D. P. Donovan (Referee #2)

The reviewer's comments are in black and our answers are in blue. Snippets of text from the submitted manuscript are in italics while modifications of the manuscript are shown in bold italics. The pages and lines reported here correspond to the submitted manuscript.

This paper describes a novel method to determine (thin) ice cloud optical depth as well as some limited mean particle size information using a combination of lidar data, IR radiometry and atmospheric thermodynamic state information. The technique appears robust and appears reasonably easy to implement. It could also be a candidate for network deployment.

The paper is, in the main, clear and well-written and worthy of publication. Another reviewer has already noted a number of issues. I have noted a further few aspects that should be improved before final acceptance.

We would like to thank Dave Donovan for his pertinent and informative comments. We provide below a point-by-point reply to his comments.

P1: line 1: What type of profile information? Please be specific here.

We have completed the missing information. P1 L1: *Multi-band downwelling thermal measurements of zenith sky radiance, along with **cloud boundary heights** ~~height profile information~~, ...*

P11: Lines 25-28: The authors should expand the lidar multiple-scattering discussion. It is not quite satisfying/convincing to me. I agree that the application of Eloranta's formalism is appropriate, (it would be useful if they specified the equation number of the formula they used) however, they must follow through to discuss the errors in terms of optical depth and not leave the discussion solely in terms of Pt/P1. Also, the discussion must be made much clearer.

For example, (looking at Eq. 4) it is clear that the important factor in determining the COD is the ratio of the signals at cloud base and cloud top. Thus, the relevant quantity for determining the effect of MS is the Pt/P1 ratio at cloud top (since at cloud-base Pt=0). However, curiously, the worst-case cloud-base height is defined as 5.5 km but the cloud top altitude is not specified.

Assuming that the worst-case Pt/P1 ratio value of 60% quoted by the authors is indeed the value at cloud-top. The error in COD induced by MS effects for the worst-case scenario can be easily calculated. Using Eq.4 it is easy to show that the effect of MS will be to lower the retrieved extinction by an amount given by

$$dCOD_{ms} = -0.5 \log (1.0+Pt/P1)$$

and Pt=0.6 P1 implies that $dCOD_{ms}= 0.23$ which is about a -10% bias.

Moving on, it is not clear what the authors mean by the "overall average value for the Pt/P1 upper limit". Is that the altitude averaged value for the just described "worst-case" scenario or the average ratio at cloud-top over the investigated cases? If the former, then it is not a useful quantity. If the latter then that would correspond to a COD retrieval bias of -0.05 which could be significant for many of the results presented in this paper (e.g. see Fig .6 before about 19:00). Indeed accounting for the MS effects may bring the IR radiometer and lidar results more into line with each other values.

The authors have enough information to define the COD, cloud geometry and particle size ranges they are dealing with. Using this information and Eloranta's model I think with not too much effort they

could define and apply a mean eta factor as was done in the paper by Platt which they reference.

Multiple-scattering (MS) is an important question and we agree that this part could be improved. The former approach (using the formula (16) in Eloranta (1998)) has been improved by using his model for all the cases (Figure 1). As Dr. Donovan correctly wrote, the MS is maximum at cloud top height (or at least, very close to top height depending on the backscatter profile) and we changed it in the text. We also pursued this study to estimate the MS coefficient, as defined in Platt (1973), to take account of the MS effects. We hope that the additional statements will help the readers to understand the real but limited (less than 10 %) impact of MS in the present cloud study.

Due to a very small angular field-of-view of the AHSRL receiver (45 μ rad) it is common to assume the molecular backscatter cross section is not affected by multiple scattered photons (Eloranta et al., 2007).

However, to better quantify the effect of multiple scattering, we applied Eloranta's (1998) approximate model to calculate the multiply scattered lidar returns for the 150 cloud cases. The inputs included molecular and particulate backscatter coefficients, effective diameters (inferred from the AHSRL+MMCR technique discussed below) and cloud height boundaries. The approximate model was employed to compute multiple scattering returns up to the 4th order. The impact of multiple scattering (MS) can then be evaluated in terms of COD inasmuch as multiple scattering lowers the apparent COD. From Equation (4), we define Δ COD_ms as :

$$\Delta\text{COD}_{ms} = -0.5 \log(1.0 + Pt/P1)$$

where Pt is an output of the MS model, representing all orders of multiple scattering while P1 is the single scattering return. This term can be used to correct the retrieved optical depth by inserting a multiplicative factor η , as per Platt (1973) to correct for the reduction of the extinction coefficient. The parameter η is not constant (Bissonnette, 2005) and Platt argued that it should vary between 0.5 and 1. Our best estimate of η over the ensemble of test cases was 0.95. This factor was used to correct the lidar-derived COD that we employed for validation purposes in this manuscript.

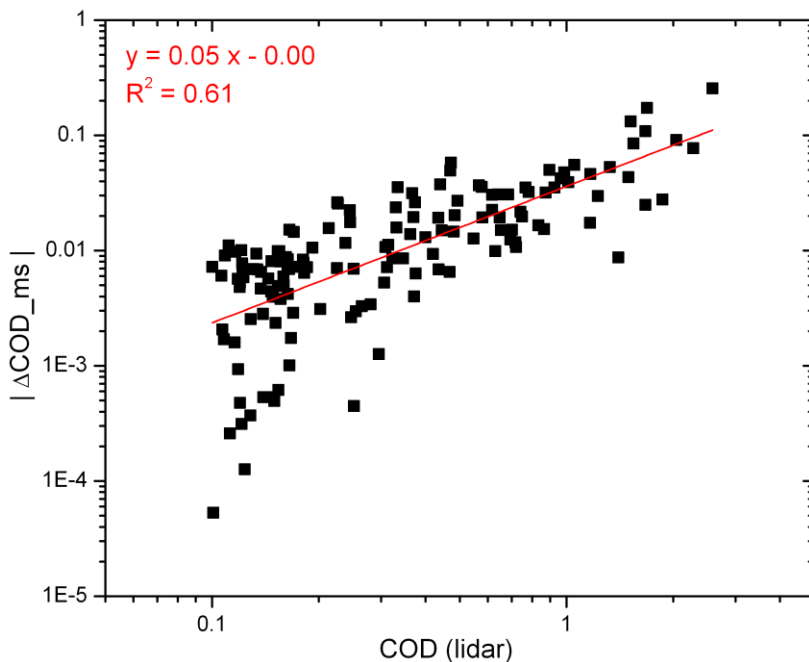


Figure 1: Difference in COD due to multiple scattering, according to the calculations of Eloranta's model (1998). The black squares represent the 150 cases selected in this study.

Page 20: Line 5-10: Can the authors please comment on how realistic it is to assume that all the measurement errors on the IR BTs are indeed independent?

From an error analysis of a very similar instrument (we used a newer version with 2 additional channels), in Legrand et al. (2000), we cannot state that the measurement errors are wavelength-independent. On the contrary, it seems that the global uncertainties for each channel depend on the detector temperature (Legrand et al, 2000; Brogniez et al., 2003).

We understand that our choice of assuming uncorrelated noise is simplistic but this assumption is done in numerous studies (e.g. Daniel et al., 2003; Turner, 2003; Sourdeval et al., 2013; Köhler et al., 2015; Sourdeval et al., 2016). We assume that the correlated errors would be reduced when the cloud dominates the measured signal (as the measured T_b is strongly linked to COD).

Some corrections can also be done to reduce noise level and therefore to minimize the off-diagonal elements of the covariance matrix. For example, a noise filter using principal component analysis was applied to P-AERI data in this study to reduce uncorrelated error (Turner et al., 2006).

Page 20: Line 14: $\sigma/\sqrt{1000}$. What is the significance of the $\sqrt{1000}$ term ?

The goal of applying the $\sqrt{1000}$ term was to have the same order of magnitude in the total error covariance matrix. By applying this term, we ensure to keep the spectral variation of the forward model errors.

References:

Brogniez, G., C. Pietras, M. Legrand, P. Dubuisson, and M. Haeffelin, 2003: A High-Accuracy Multiwavelength Radiometer for In Situ Measurements in the Thermal Infrared. Part II: Behavior in Field Experiments. *J. Atmos. Oceanic Technol.*, 20, 1023–1033, doi: 10.1175/1520-0426(2003)20<1023:AHMRFI>2.0.CO;2.

Bissonnette, L. R., 2005: Lidar and multiple scattering. *Lidar Range-Resolved Optical Remote Sensing of the Atmosphere*, C. Weitkamp, Ed., Springer, 43–104

Daniel, J. S., S. Solomon, H. L. Miller, A. O. Langford, R. W. Portmann, and C. S. Eubank, Retrieving cloud information from passive measurements of solar radiation absorbed by molecular oxygen and O₂-O₂, *J. Geophys. Res.*, 108(D16), 4515, doi:10.1029/2002JD002994, 2003.

Eloranta, E. W, Practical model for the calculation of multiply scattered lidar returns, *Appl. Opt.* 37, 2464-2472, 1998

Köhler, P., Guanter, L., and Joiner, J.: A linear method for the retrieval of sun-induced chlorophyll fluorescence from GOME-2 and SCIAMACHY data, *Atmos. Meas. Tech.*, 8, 2589-2608, doi:10.5194/amt-8-2589-2015, 2015.

Legrand, M., C. Pietras, G. Brogniez, M. Haeffelin, N. Abuhassan, and M. Sicard, 2000: A High-Accuracy Multiwavelength Radiometer for In Situ Measurements in the Thermal Infrared. Part I: Characterization of the Instrument. *J. Atmos. Oceanic Technol.*, 17, 1203–1214, doi: 10.1175/1520-0426(2000)017<1203:AHAMRF>2.0.CO;2.

Platt, C., 1973: Lidar and Radiometric Observations of Cirrus Clouds. *J. Atmos. Sci.*, 30, 1191–1204, doi: 10.1175/1520-0469(1973)030<1191:LAROOO>2.0.CO;2.

Sourdeval, O., Labonnote, L. C., Brogniez, G., Jourdan, O., Pelon, J., and Garnier, A.: A variational approach for retrieving ice cloud properties from infrared measurements: application in the context of two IIR validation campaigns, *Atmospheric Chemistry and Physics*, 13, 8229–8244, doi:10.5194/acp-13-8229-2013, <http://www.atmos-chem-phys.net/13/8229/2013/>, 2013.

Sourdeval, O., C.-Labonnote, L., Baran, A. J. and Brogniez, G. (2015), A methodology for simultaneous retrieval of ice and liquid water cloud properties. Part I: Information content and case study. *Q.J.R. Meteorol. Soc.*, 141: 870–882. doi:10.1002/qj.2405

Turner, D.D., 2003: Microphysical properties of single and mixed-phase Arctic clouds derived from ground-based AERI observations. Ph.D. Dissertation, University of Wisconsin - Madison, Madison, Wisconsin, 167 pp.

Turner, D. D., Knuteson, R. O., Revercomb, H. E., Lo, C., and Dedecker, R. G.: Noise Reduction of Atmospheric Emitted Radiance Interferometer (AERI) Observations Using Principal Component Analysis, *J. Atmos. Oceanic Technol.*, 23, 1223–1238, doi:10.1175/JTECH1906.1, <http://dx.doi.org/10.1175/JTECH1906.1>, 2006.

Response to Anonymous Referee #3

The reviewer's comments are in black and our answers are in blue. Snippets of text from the submitted are in italics while modifications of the manuscript are shown in bold italics. The pages and lines reported here correspond to the submitted manuscript.

This paper reports on the development and testing of new LIRAD method that utilizes thermal infrared bands available on the CIMEL CE-312 radiometer, which is considerably cheaper than the AERI. The latter has been used in the recent past to provide the thermal components to retrieve COD and D_{eff} from the surface. The implicit motivation for this study seems to be that the LIRAD method can be used more often if the CIMEL-312 could be used instead of the AERI, since it is attempting to do the same things that AERI already provides. The explicit motivation is that the ability to discriminate between small and large D_{eff} values would help the study of aerosol/cloud interactions in polar regions, especially regarding aerosol influence on precipitative cooling and (as inferred from the DLCRF computations) on radiative heating of the surface. The writing is of average quality, but has some grammatical issues. The paper is scientifically sound in its approach, but the results and method do not appear to be particularly new.

We are grateful to this reviewer for the helpful comments. We provide below a point-by-point reply to his comments.

The algorithm is new in that it uses specific bands not previously employed in the AERI-LIRAD approach. However, they are not all that different from the AERI microwindows. Except for lacking the wavelengths longer than 14 μm , this is essentially the same algorithm. If not, then it needs more contrasting with the MIXCRA. It relies on the phase being known already, whereas, I believe, the longer wavelengths used in the MIXCRA were primarily for phase discrimination. It is not surprising then that the results are quite close to those from the MIXCRA. The bottom line that I believe the authors should address is “how many wavelengths are actually needed to replace the 19 microwindows of MIXCRA having $\lambda < 13 \mu\text{m}$ to perform the retrieval?” Could you do it with 2 or 3 channels? There appears to be a lot of information redundancy in the bands that were used.

The question about information redundancy is pertinent. We believe the information in section 4 (the discussions centered on Figures 2, 3 and 4) shows the sensitivity of each band to the key radiative transfer parameters and therefore helps to demonstrate the importance of those bands. The T_b separation of the spectral curves in Figures 3a and 3b is a progressively damped out sensitivity to the cold-space temperature that is essentially controlled by water vapour absorption at $\text{COD} = 0$. The variation of the brightness temperature with D_{eff} in Figure 3b is reflective of essentially two dominant optical mechanisms juxtaposed on the progressive warming of the cold background : (i) the classical increase in the extinction efficiency with increasing D_{eff} (and, optically speaking, with decreasing wavelength) in what we call the small-particle Angstrom-exponent region and (ii) the filtering / masking of this robust monotonicity (linearity on a log-plot) caused by significant variations in the real and complex parts of the refractive index in the last 3 bands (notably the last 2 bands). This translates, in a 1st order sense, to an Angstrom type of slope requirement for at least 2 short wavelength bands (3 for better redundancy). The monotonic dependence of brightness temperature as a function of COD in Figure 3a is also dependant on the interplay of the 2 extinction efficiency influences and the progressive warming of the cold-space temperature. It is clear that any single band would fare quite well in a T_b inversion to extract COD but that the most transparent bands to water vapour would be more sensitive (the 11.3 μm band in Figure 3a). As the brightness temperature of all bands is also sensitive to a variety of parameters (Figure 4), it is important, we believe, to maintain a certain redundancy in order to ensure a

robust retrieval.

To further support this answer to the reviewer's question, we performed retrievals with different band configurations and compared retrieval statistics for the COD and D_{eff} retrievals (tables below). The order of the elimination of these bands was based on a progressive increase in per-band information content (roughly from minimum to maximum dX / dT_{b_i} where $X = \text{COD}$ or D_{eff} and where T_{b_i} is the brightness temperature for band i in the region of greatest sensitivity to X)

Table 1: Retrieval statistics for different band configurations.

Bands used (μm)	COD retrieval (R^2 – RMS Errors)	Deff retrieval (overall accuracy)
8.4, 8.7, 9.2, 10.7, 11.3, 12.7	0.95 – 0.09	83%
8.7, 9.2, 10.7, 11.3, 12.7	0.95 – 0.09	75%
9.2, 10.7, 11.3, 12.7	0.95 – 0.09	72%
10.7, 11.3, 12.7	0.95 – 0.09	71%
10.7, 11.3	0.95 – 0.09	74%
11.3	0.95 – 0.09	69%

Bands used (μm)	COD retrieval (R^2 – RMS Errors)	Deff retrieval (overall accuracy)
8.4, 8.7, 9.2, 10.7, 11.3, 12.7	0.95 – 0.09	83%
8.4, 8.7, 9.2, 10.7, 11.3	0.95 – 0.09	81%
8.4, 8.7, 9.2, 10.7	0.95 – 0.09	77%
8.7, 9.2, 10.7	0.95 – 0.10	73%
8.7, 9.2	0.94 – 0.11	67%
9.2	0.94 – 0.11	67%

The COD retrieval statistics are similar even if only one band is used in the retrieval algorithm (where that one band is the most T_b sensitive, 11.3 μm band). In the case of the D_{eff} retrieval, the overall accuracy decreases slowly until the Angstrom slope information is eliminated by reducing the band number from 2 to 1.

The validation effort includes the comparisons with MIXCRA (noted above) and with lidar for COD. This begs the question: If the lidar is required for the LIRAD method and it produces a reliable COD (it is used as a reference), why then is the IR method used to estimate COD? Why not simply estimate D_{eff} using the IR data and the lidar COD as input? Lidar retrievals of COD are quite common for most lidars deployed for surface observations. What am I missing? How will phase be determined if this approach is implemented elsewhere?

The radiometer is designed to be a portable instrument and can be easily deployed to a remote station. We could certainly use the lidar COD as input but the requirement for applying our retrieval method is only cloud base altitude information (and ideally also cloud thickness). This could be obtained from a ceilometer or a portable, low-power lidar (CE370 LiDAR from CIMEL, for example). Put another way, the advanced capabilities of a lidar such as the AHSRL were needed for the validation but only a ceilometer was required to estimate the required input parameters to our passive retrieval algorithm (the

AHSRL is overkill in the latter case).

We inserted the following sentences in the conclusion of the paper: P.20 L.12 *An important application of our work would be to deploy this technique as part of a network of low-cost and robust instruments to monitor Arctic clouds. Because their occurrence, type and altitude are spatially inhomogeneous (according to Eastman and Warren (2010) and Shupe et al. (2011)), we believe that additional ground-based stations would be helpful to broaden our knowledge of arctic ice clouds.*

Some authors have proposed to use the absorption coefficient differences between 10 and 13 μ m for phase discrimination (ice being absorbing than water; see, for example, Baum et al., 2000). However, inasmuch as absorption is also a function of particle size (see Fig. 2), it could be difficult, to separate ice and water in the case of small particles (Turner, 2003). This is why the bands between 16 and 20 μ m are used in the case of MIXCRA.

Moreover, as shown by Shupe (2011), the frequency of liquid clouds (either liquid-only or mixed-phase clouds) is low at Eureka (annual average of 30%, mainly occurring in the summer and autumn and below 20% during the wintertime, when the cases in this study were chosen).

I think this paper can be published, but it needs some major revisions to provide better justification as to why it is necessary and to flesh out the analysis by addressing the questions above.

Minor comments

P1, L24: “temperatures” does not belong here

It has been removed.

P3, L4: “ aerosols acting as ice and water cloud nuclei, cloud microphysics, precipitation and radiation” does not make any sense. Please reorder this so that aerosols do not appear to act as cloud microphysics.

This sentence was rewritten: P3 L4 : *Much of the recent research has been focused on aerosol-cloud interactive processes involving aerosols acting as ice and water cloud nuclei **and their subsequent affect on** cloud microphysics, precipitation and radiation.*

P3, L14: You may want to modify the sentence with "could possibly lead to" or something similar, since the “dehydration greenhouse feedback” is only a proposed mechanism.

This sentence was rewritten as suggested: P3 L14 : *In terms of the purpose and motivation for this paper, we note that the presence of sulphuric-acid bearing aerosols (viz., Arctic haze) can significantly increase the size of ice particles (relative to the size of ice particles formed from more pristine, low acid aerosols or supercooled droplets). This process can ~~cause-leading~~ enhanced precipitation and important cooling effects during the polar winter **and could possibly lead to a dehydration greenhouse feedback (DGF) effect, as proposed by Blanchet and Girard (1994).***

P4, L3: Please “COD” for singular and “CODs” or “COD values” for plural here and throughout the paper

The consistency of the use of the singular and plural forms was corrected in the paper.

P4, L9: “northern most” should be one word

Corrected.

P4, L14: if the same summary is given by both references, then leave one out. If two different summaries are provided, then change everything to the plural form.

We chose to keep the reference of Bourdages et al. (2009) as the technical specifications were more detailed.

P4, L17: “in the order of” should be “on the order of”

Corrected.

P5, L24-25: The <2% refers only to downwelling radiation viewed at the zenith. It can be up to 10% for other viewing conditions, particularly for upwelling radiation (e.g., Minnis et al., JAS 93). The viewing limitation should be highlighted again when referring to the 2%.

We have added this correction: P5 L24: *Platt (1973) and later authors such as Turner and Lohnert (2014) indicated that only a small fraction of the zenith-looking downwelling radiation emitted by a cloud was due to scattering.*

P7, L16: COD can only have an amplitude if you are referring to its oscillation with time or space. Otherwise, please refer to it as magnitude or value.

That is true, we were talking about its magnitude. P7, L16: *At COD magnitudes ~~amplitudes~~ greater than 2-3, ...*

P8, L3-6: Sentence should be broken up for clarity.

The rewritten sentences are: P8 L3-L6: *The simulation results in Figure 4 detail the band dependent effects of six different parameters by comparing changes in T_b induced by each parameter individually. These were obtained for 1000 appropriately normalized samples of a random number generator with a normal probability distribution whose mean and standard deviation was controlled by the six parameter values of Table 2 (COD, D_{eff} , cloud base height, cloud thickness, column integrated water vapor of the atmosphere (WVC) and particle shape).*

P8, L16: cloud altitude and thickness uncertainties do not have amplitudes in this context. See comment above.

It was corrected. P8 L16: *If the altitude and the thickness of the clouds are known from vertical lidar (and radar) profiles then the **magnitude** ~~amplitude~~ of the altitude and cloud thickness uncertainties of Figure ...*

P10, L1: Here and elsewhere, the form of the modifier does not need to match that of the noun. Should be “ice cloud retrievals”.

Corrected.

P11, L10: “mean’t” appears to be a typo.

Corrected.

P12, L12: “produces gives”, please use one or the other

We removed “produces”.

P12, L18: should be “hydrometeor diameter”

Corrected.

P16, L4-5: “ommission” has only one “m”

Corrected.

References:

Baum, B. A., P. F. Soulen, K. I. Strabala, M. D. King, S. A. Ackerman, W. P. Menzel, and P. Yang, 2000: Remote sensing of cloud properties using MODIS airborne simulator imagery during SUCCESS: 2. Cloud thermodynamic phase, *J. Geophys. Res.*, 105(D9), 11781–11792, doi:10.1029/1999JD901090.

Eastman, Ryan, Stephen G. Warren, 2010: Arctic cloud changes from surface and satellite observations. *J. Climate*, 23, 4233–4242. doi: 10.1175/2010JCLI3544.1

Shupe, M.D., 2011: Clouds at Arctic Atmospheric Observatories, Part II: Thermodynamic phase characteristics. *J. Appl. Meteor. Clim.*, 50, 645-661.

Turner, D.D., 2003: Microphysical properties of single and mixed-phase Arctic clouds derived from ground-based AERI observations. Ph.D. Dissertation, University of Wisconsin - Madison, Madison, Wisconsin, 167 pp. Available from <http://www.ssec.wisc.edu/library/turnerdissertation.pdf>

Turner, D. D. and U. Löhnert, 2014: Information Content and Uncertainties in Thermodynamic Profiles and Liquid Cloud Properties Retrieved from the Ground-Based Atmospheric Emitted Radiance Interferometer (AERI). *J. Appl. Meteor. Climatol.*, 53, 752–771, doi: 10.1175/JAMC-D-13-0126.1

Thin ice clouds in the Arctic: Cloud optical depth and particle size retrieved from ground-based thermal infrared radiometry

Yann Blanchard¹, Alain Royer¹, Norman T. O'Neill¹, David D. Turner², and Edwin W. Eloranta³

¹Centre d'Applications et de Recherches en Télédétection, Université de Sherbrooke, Sherbrooke, Québec, Canada.

²Global Systems Division, Earth System Research Laboratory, National Oceanic and Atmospheric Administration, Boulder, Colorado, USA.

³Space Science and Engineering Center, University of Wisconsin, Madison, Wisconsin, USA.

Correspondence to: Yann Blanchard (yann.blanchard@usherbrooke.ca)

Abstract. Multi-band downwelling thermal measurements of zenith sky radiance, along with cloud boundary heights, were used in a retrieval algorithm to estimate cloud optical depth and effective particle diameter of thin ice clouds in the Canadian high-Arctic. Ground-based thermal infrared (IR) radiances for 150 semi-transparent ice clouds cases were acquired at the Polar Environment Atmospheric Research Laboratory (PEARL) in Eureka, Nunavut, Canada (80°N, 86°W). We analyzed and quantified the sensitivity of downwelling thermal radiance to several cloud parameters including optical depth, effective particle diameter and shape, water vapor content, cloud geometric thickness, and cloud base altitude. A look up table retrieval method was used to successfully extract, through an optimal estimation method, cloud optical depth up to a maximum value of 2.6 and to separate thin ice clouds into two classes: 1) TIC1 clouds characterized by small crystals (effective particle diameter ≤ 30 μm), and 2) TIC2 clouds characterized by large ice crystals (effective particle diameter > 30 μm). The retrieval technique was validated using data from the Arctic High Spectral Resolution Lidar (AHSRL) and Millimeter Wave Cloud Radar (MMCR). Inversions were performed across three polar winters and results showed a significant correlation ($R^2 = 0.95$) for cloud optical depth retrievals and an overall accuracy of 83% for the classification of TIC1 and TIC2 clouds. A partial validation relative to an algorithm based on high spectral resolution downwelling IR radiance measurements between 8 and 21 μm was also performed. It confirms the robustness of the optical depth retrieval and the fact that the broadband thermal radiometer retrieval was sensitive to small particle (TIC1) sizes.

1 Introduction

Predictions of future climate change and its regional and global impacts require that a better understanding of the radiative transfer interactions between clouds, water vapor and precipitation be incorporated into appropriate models. Recent CMIP5 model intercomparisons (the Coupled Model Intercomparison Project as described in Jiang et al., 2012) indicate large variability in ice cloud parameters (for example ice water content) amongst high-latitude models. Shortcomings in ice cloud parametrization (Baran, 2012) impact their representation of radiative effects as well as water cycles and leads to uncertainties in quantifying cloud feedbacks in the context of climate change (Waliser et al., 2009). High-altitude thin ice clouds consisting of pure ice crystals, which cover between 20 to 40% of the Earth (Wylie and Menzel, 1999), can, for example, have opposing

effects on the radiative properties of the Earth. A surface cooling effect ensues when scattering by clouds reduces the solar radiation reaching the Earth's surface (i.e., albedo effect). By contrast, a reduction in the amount of IR energy escaping the Earth-atmosphere system occurs when the upwelling IR radiation emitted by the Earth's surface and lower atmosphere is absorbed by clouds and radiated back downward (i.e., greenhouse effect) (Stephens and Webster, 1981). The macrophysical and microphysical properties of thin ice clouds determine which process dominates and hence determine the net forcing of thin ice clouds on the climate system (Stephens, 2005). The optical properties of thin ice clouds can be represented by extensive parameters such as the optical depth and ice water content as well as intensive parameters such as ice crystal size and shape. In an Arctic environment, the radiative effects of ice clouds are unique because their radiative forcing influence on the energy balance depends on seasonal Polar day to Polar night variation as well as large scale processes like the Arctic Oscillation (Wang and Key, 2003). The advent of active sensors onboard satellites (for example CALIPSO/CloudSat) has enabled the application of considerably more resources for polar region ice cloud studies. This permits the evaluation of climate models (Jiang et al., 2012) and satellite cloud climatologies (Sassen et al., 2008). Long-term ground-based observations which are also essential for the validation of models and satellite climatology are, however, limited in their Arctic coverage (Heymsfield et al., 2017). Thermal IR radiometry is a well-known technique for investigating the presence and the emissivity of clouds (Allen, 1971). Numerous researchers have exploited the thermal IR behavior of the absorption and scattering efficiencies of cloud particles as a means of retrieving CODs and particle effective sizes (e.g., Inoue, 1985). As cloud altitudes (temperatures) can lead to large uncertainties in this latter technique, Platt (1973) proposed using lidar backscatter profiles along with IR radiometry to estimate cloud altitudes and accordingly improve the retrieval accuracy of cloud emissivity. This active/passive technique (called LIRAD for lidar/radiometer method by Platt) has evolved over the years with such improvements as the availability of high resolution spectrometers (Smith et al., 1993; Lubin, 1994). The LIRAD technique is based on spectral radiance/brightness temperature comparisons between measurements and radiative transfer calculations. It performs better in the presence of high thermal contrast and is thus well suited for cloud retrievals (Lubin, 1994). In more recent applications, cloud optical depth, effective radius and ice fraction were retrieved from AERI (Atmospheric Emitted Radiance Interferometer; Knuteson et al., 2004a, b) spectral downwelling radiance observations in Antarctic, during the Surface Heat Budget of the Arctic Ocean (SHEBA) campaign and ARM North Slope of Alaska site (Turner et al., 2003; Shupe et al., 2015; Mahesh et al., 2001, respectively). The Turner (2005) method was also employed at Eureka (Nunavut, Canada) to retrieve cloud optical depth and cloud microphysical parameters from AERI spectra acquired between 2006 and 2009 (Cox et al., 2014). A proposed satellite-based instrument whose goal will be the characterization of thin ice clouds in the Arctic using far and thermal infrared channels (Blanchet et al., 2011) was recently tested during an airborne campaign in the High Arctic (Libois et al., 2016).

In this paper, we examine how multi-band thermal measurements of zenith sky radiance can be used to retrieve what are, as indicated in the early remote sensing literature (see Nakajima and King, 1990, for example), the most critical extensive and intensive parameters influencing the radiative effects of ice clouds: cloud optical depth (COD) and effective particle diameter (D_{eff}). We propose an application of this LIRAD technique with a relatively simple and inexpensive instrument (less than 10% of the cost of an AERI) that is well-suited to the Arctic environment (Royer et al., 2014). Inasmuch as ice particle size is difficult to retrieve from IR radiometry, the D_{eff} component of our retrievals will be focused on a simple discrimination of

large and small crystal sizes. This approach was motivated by previously published research that indicated such a discrimination would play a key role in characterizing an important aerosol/cloud interaction process in Polar winter, namely precipitative cooling (see, for example, Blanchet and Girard, 1994; Grenier et al., 2009). An important aspect in this paper is that our COD and D_{eff} retrievals will be validated using independent lidar and radar retrievals.

5

Section 2 highlights the importance of studying ice clouds while Section 3 is devoted to the description of the study site and instrumentation. Section 4 examines the sensitivity of thermal IR radiometry to key ice cloud parameters. In Section 5 we describe and verify the proposed methodology for retrieving COD and D_{eff} using thermal IR radiometry measurements. The results are presented and discussed in Section 6 for the 150 thin ice clouds cases we observed in the Arctic.

10 2 Classification and Parameterization of Thin Ice Clouds

Water vapor and clouds are a significant climate modeling challenge since they represent major radiative forcing influences, while being the least understood components of the climate system (Waliser et al., 2009; Jiang et al., 2012). Much of the recent research has been focused on aerosol-cloud interactive processes involving aerosols acting as ice and water cloud nuclei and their subsequent affect on cloud microphysics, precipitation and radiation (see for example, Feingold and McComiskey (2016) on recent ARM campaigns, Winker et al. (2010) and Illingworth et al. (2015) respectively, on the cloud remote sensing mandate of the A-Train and EarthCARE satellite missions and Jouan et al. (2014) as part of the NETCARE project). In particular, understanding aerosols and their radiative effects, especially their indirect impacts as cloud condensation nuclei, is of critical importance for climate change models. The indirect effect of aerosols represents a cooling influence (whose amplitude is subject to large uncertainties) on the global radiative budget (Intergovernmental Panel on Climate Change, IPCC, 2013). The estimated uncertainty of the indirect forcing component (between -0.1 and -1.3 W.m^{-2}) is associated with variations in cloud properties and cloud lifetime. In the Arctic, the nature of thin ice clouds can effectively induce an indirect cooling influence given the proper conditions. In terms of the purpose and motivation for this paper, we note that the presence of sulphuric-acid bearing aerosols (viz., Arctic haze) can significantly increase the size of ice particles (relative to the size of ice particles formed from more pristine, low acid aerosols or supercooled droplets). This process can cause enhanced precipitation and important cooling effects during the polar winter and could possibly lead to a dehydration greenhouse feedback (DGF) effect, as proposed by Blanchet and Girard (1994).

The small and large ice particles described above are often abbreviated as TIC1 and TIC2 (thin ice cloud, type 1 and 2). Thin ice cloud classification was carried out by Grenier et al. (2009) using the active techniques of lidar and radar: CALIPSO and CloudSat data were employed to discriminate between TIC1 and TIC2 ice clouds using the CloudSat small-particle sensitivity minimum of approximately $30\text{-}40 \mu\text{m}$. In this study, we seek to demonstrate that TIC1 and TIC2 discrimination can be determined using zenith-looking IR radiance measurements acquired at the Eureka observatory in the Canadian High Arctic. Figure 1 illustrates lidar and radar backscatter profiles acquired at Eureka for distinct TIC1 and TIC2 cases.

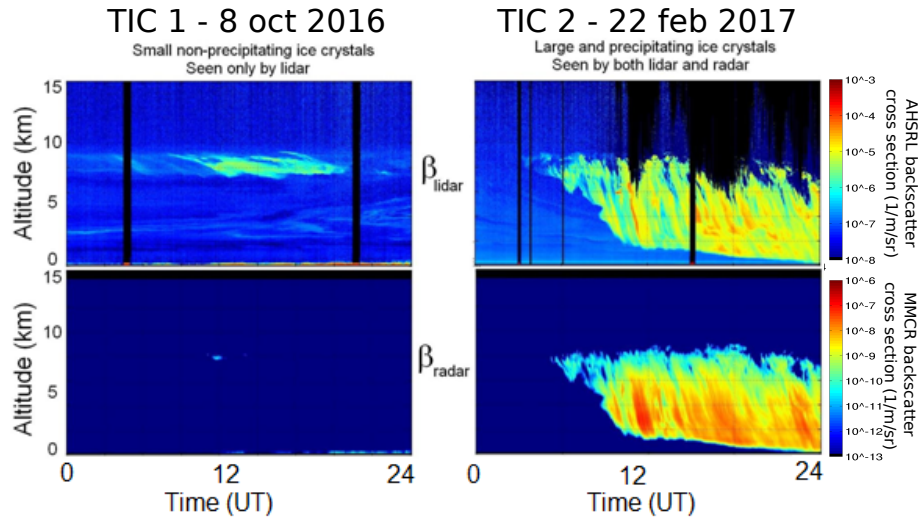


Figure 1. Classification of thin ice clouds using ground-based lidar (up) and radar backscatter profiles (bottom).

The left hand lidar profile of Figure 1 shows a TIC that is largely transparent to cloud radar while the right hand lidar profile shows a thin ice cloud that is readily detected by the radar. The disparity in radar detectivity enables one to conclude that the former case corresponds to a small-particle TIC1 event while the latter case corresponds to a large-particle TIC2 event.

The presence or absence of thin ice clouds in the winter can lead to significant changes in surface cooling (Stephens et al., 1990). Given the important radiative influence of ice crystal size and COD it is necessary that these parameters be well-characterized in order to improve modeling of their radiative effects (Ebert and Curry, 1992) and thus their influence within a context of TIC1 and TIC2 clouds.

The effective diameter of atmospheric ice particles is defined by Hansen and Travis (1974):

$$D_{eff} = \frac{3V}{2A} \quad (1)$$

where A and V are respectively the total projected area and volume of all ice particles per unit surface area in a given atmospheric column (Baum et al., 2014). COD is given by:

$$COD = \int \pi Q_{ext} \frac{D^2}{4} a(D) dD \quad (2)$$

where Q_{ext} is the extinction efficiency (extinction cross section per unit projected-particle-area) (Hansen and Travis, 1974), D is the particle diameter and $a(D)$ is the ice particle number density per unit increment in diameter. We note that, while the lidar-derived CODs employed in this article are at $0.532 \mu\text{m}$, the IR CODs from our retrieval method were referenced, for convenience, to $0.55 \mu\text{m}$ (we assume that COD differences between 0.532 and $0.55 \mu\text{m}$ are negligible within the context of other uncertainties encountered in this study).

Table 1. List of the Eureka (PEARL) instruments employed in our analysis.

Ground-based instrument	Duty cycle	Research group or institution
AHSRL (Arctic High Spectral Resolution Lidar)	Continuous	SEARCH/NOAA - U. of Wisconsin
MMCR (Millimeter Cloud Radar)	Continuous	SEARCH/NOAA - ARM
Radiosonde	Twice a day	Environment Canada
P-AERI (Polar-AERI)	Continuous (except during precipitation)	SEARCH/NOAA - U. of Idaho

3 Study site and instrumentation

The observation site was the Polar Environment Atmospheric Research Laboratory (PEARL) in Eureka, Nunavut (80°N, 86°W) which is one of the high-latitude stations of the Network for the Detection of Atmospheric Composition Change (NDACC, http://www.ndsc.ncep.noaa.gov/sites/stat_reps/eureka/). This high Arctic site is located in the northernmost part of the Canadian Arctic Archipelago. It was chosen because of our interest in Arctic ice clouds and to exploit the diverse and complementary inventory of atmospheric instruments listed in Table 1 (i.e., lidar, radar, IR spectrometer and radiosondes), as well as the infrastructure and logistics support for field campaigns.

Detailed descriptions of the AHSRL and MMCR data processing and interpretative techniques can be found in Eloranta (2005) and Moran et al. (1998). A summary of instrument specifications is given in Bourdages et al. (2009). Knuteson et al. (2004a, b) present a discussion of the AERI performance which is applicable to the present paper. The AERI instrument is known to have a very small warm bias for low radiance measurements, typically for clear-sky events, on the order of 1% of the ambient radiance (Knuteson et al., 2004b; Delamere et al., 2010). As the focus of our work is on clouds with COD greater than 0.1, this warm bias in the AERI has only a slight to negligible impact for retrievals involving very thin clouds (Turner, 2003). The AERI data used in this work have been post-processed to reduce the uncorrelated random error in the data using principal component analysis (Turner et al., 2006).

In this paper, we focus on the potential of using data from a ground-based multi-band thermal radiometer, the CIMEL CE-312 developed by CIMEL Inc (see Legrand et al., 2000; Brogniez et al., 2003, for descriptions of a similar instrument). The 6 channels of this radiometer correspond to (full width at half maximum) limits of 8.2-8.6, 8.5-8.9, 8.9-9.3, 10.2-10.9, 10.9-11.7 and 11.8-13.2 μm and filter response peak values at 8.4, 8.7, 9.2, 10.7, 11.3 and 12.7 μm . The multi-band radiometer is also a robust instrument, that, unlike the AERI, does not require a thermally controlled environment. In actual fact however, we had to simulate the response of this radiometer by convolving the spectral transmittance of each filter with the spectra of the Eureka Polar AERI (P-AERI) instrument (provided by Von Walden at the U. of Idaho and NOAA). The reason for this was that the CIMEL radiometer that we hoped to use was not ready for deployment when we performed the field campaigns.

4 Sensitivity of Thermal Infrared Radiometry to Thin Ice Clouds

The spectral sensitivity of longwave (thermal) radiation to the microphysical properties of ice clouds has been investigated for satellite data (Chiriaco et al., 2004; Dubuisson et al., 2008), airborne data (Brogniez et al., 2004; Libois et al., 2016) and ground-based sensors (e.g. Comstock and Sassen, 2001; Yang et al., 2005, and articles cited above). Previous studies have demonstrated that thermal IR radiometry is relevant in terms of permitting the retrieval of both COD and, to a degree, D_{eff} . The retrieval of the latter parameter permits, in turn, a discrimination of TIC1 and TIC2 clouds. The dependence of thermal IR radiometry on ice particle size is represented by equation (2). The extinction efficiency, a measure of particle attenuation (absorption and scattering), depends on particle size, composition and shape as well as wavelength (Hansen and Travis, 1974). It is common, in the case of zenith-looking thermal IR (8-14 μm) radiometry of ice clouds, to neglect the scattering portion of Q_{ext} (where $Q_{ext} = Q_{abs} + Q_{sca}$), especially for large particles (Platt, 1973). The result in the presence of a medium such as cloud is extremely simplified radiative transfer that is characterized by a strong forward-scattering phase function: in the limit of a delta-function phase function, all forward scattered radiation in any given direction of incidence is returned to the incident beam and the only radiance loss is due to absorption (see, for example, the delta-function irradiance solution of Meador and Weaver, 1980). Platt (1973) and later authors such as (Turner and Löhnert, 2014) indicated that only a small fraction of the zenith-looking downwelling radiation emitted by a cloud was due to scattering (in spite of the fact that $Q_{sca} \approx Q_{abs}$).

We accordingly chose to plot absorption efficiency spectra in Figure 2 in order to illustrate the spectral sensitivity of this key radiative transfer parameter. The absorption efficiency of TIC1 particles (D_{eff} from 10 to 30 μm) and TIC2 particles (D_{eff} from 35 to 120 μm) for "severely roughened solid column" type crystals (Figure 2a and 2b) were obtained from calculations reported by Yang et al. (2013) and Baum et al. (2014). These spectra were then replaced by their mean and standard deviation across the two (TIC1 and TIC2) D_{eff} regimes in order to better appreciate the band to band separability of the TIC1 and TIC2 size classes (Figure 2c). Prior to computing those means and standard deviations of Figure 2c, we integrated the individual spectra of Figures 2a and 2b across the pass-bands of the six channels employed in this study (triangles in Figure 2c). The D_{eff} ranges employed to define TIC1/TIC2 particles, for the averaging carried out in the creation of Figure 2c, were, as in Grenier et al. (2009), roughly based on their non-detectability to detectability threshold in radar backscatter returns.

This coarse spectral representation obtained for the 6 band averages and standard deviations enables one to better appreciate the more robust nuances between the two families of spectral curves (especially for the 8.4, 8.7, 9.2 and 12.7 μm channels) and better understand the key discriminatory elements of the classification into TIC1 and TIC2 clouds. It is clear from Figure 2c that the first 4 bands offer the greatest potential for discriminating particle size. Figures 2a and 2b however indicate a decreasing sensitivity to increasing particle size as one approaches D_{eff} values in the tens of μm .

We simulated the influence of COD and D_{eff} variations, on brightness temperature (T_b) variations, using the MODTRAN 4 radiative transfer model (Berk et al., 1999). Figure 3 shows simulated T_b variations for the six radiometer channels as a function of COD for fixed D_{eff} and as a function of D_{eff} for fixed COD. The fixed values of D_{eff} and COD (and other independent parameters of the MODTRAN 4 runs) correspond to a reference case whose parameters are defined in Table 2. We chose the input parameters of the reference case as the set of mean parameters obtained by averaging over the parameters

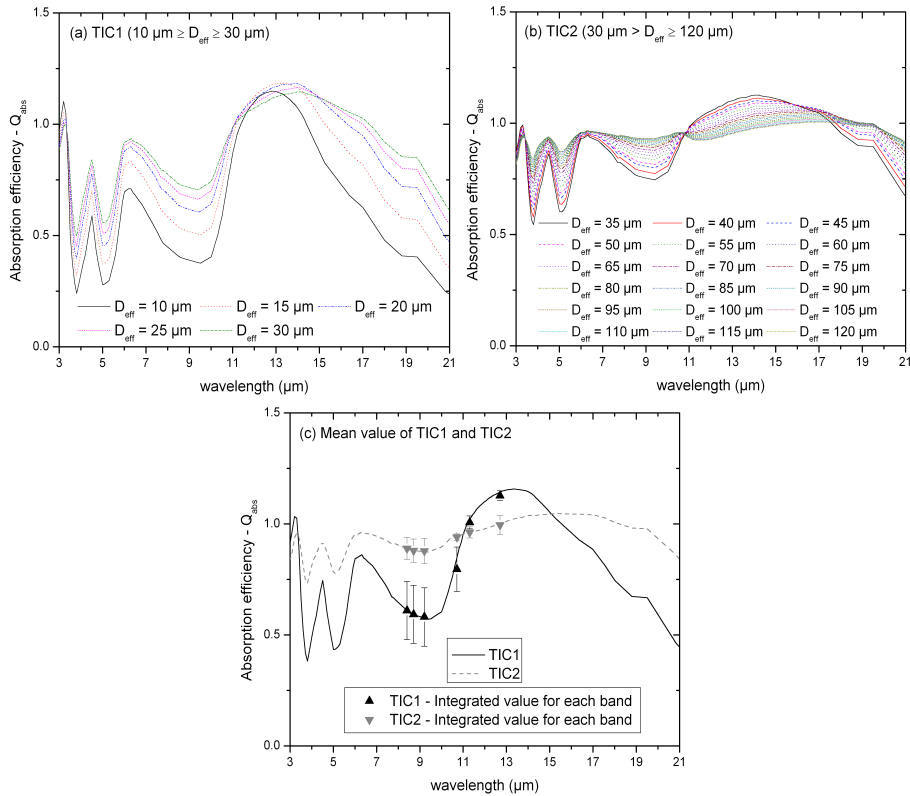


Figure 2. 2a and 2b - Absorption efficiency spectra for TIC1 and TIC2 particles across a range of D_{eff} values, 2c - Mean absorption efficiency and standard deviations across the spectra of Figures 2a and 2b. The triangular symbols represent the integration of the absorption efficiency across the six bands of the CIMEL CE-312. **These efficiencies were derived for the "severely roughened solid column" type crystals of Yang et al. (2013) and Baum et al. (2014), available at: http://www.ssec.wisc.edu/ice_models/polarization.html**

of the 150 cloud cases that we employed to provide an empirical validation of our retrieval (see Section 6.2 and Table 2 for more details). The curves of Figure 3 represent an illustrative subset of our inversion lookup table (LUT) that we employed as a means of retrieving COD and D_{eff} from measured values of T_b . The D_{eff} column is biased by the fact that the lidar-radar retrieval is insensitive to TIC1 particles: the D_{eff} reference value was accordingly biased downward to roughly overcome this insensitivity. The value of 50 μm was also the value employed by Sourdeval et al. (2013).

Figure 3a indicates that, at a fixed D_{eff} value of 50 μm , there is a strong and monotonic variation in T_b as a function of COD for all channels. At COD magnitudes greater than 2-3, the T_b values for all channels converge towards an asymptotic ceiling that is the brightness temperature of an opaque representation of the cloud. This clearly shows that the sensitivity of the method decreases progressively as the COD increases beyond 3.

Differences in T_b behavior over a range of D_{eff} values and a fixed COD of 0.5 can be observed in Figure 3b. For the channels of nominal wavelength less than 10.7 μm , T_b varies monotonically with D_{eff} up to approximately 30 μm , after which

Table 2. Average, standard deviation, maximum and minimum values of the parameters of the cloud cases used in this study. The reference case, defined in the last row, was employed to produce Figure 3 (while varying D_{eff} and the COD) and was used for the sensitivity study of Figure 4. The means, standard deviations and extrema of each parameter were derived from our analysis of the 150 cloud cases. **For the reference case, the cloud base height and thickness values were, for the sake of convenience, rounded to the nearest incremental step of the MODTRAN vertical layer profiles.**

	Cloud base height (km)	Thickness (km)	Water vapor content (g/cm^2)	COD (lidar)	Deff (μm) (lidar-radar)	Ice particle shape (3 sets of models)
Average	5.19	2.30	0.19	0.46	91.06	-Solid columns
Std Dev	2.05	1.62	0.09	0.48	25.16	-Aggregate of solid columns
Max	9.00	8.00	0.85	2.60	158.26	-A mixture involving a set
Min	0.80	0.20	0.08	0.10	40.07	of 9 habits
Reference case	5.20	2.20	0.19	0.50	50.00	Solid columns

A full description of the models can be found at http://www.ssec.wisc.edu/ice_models/polarization.html

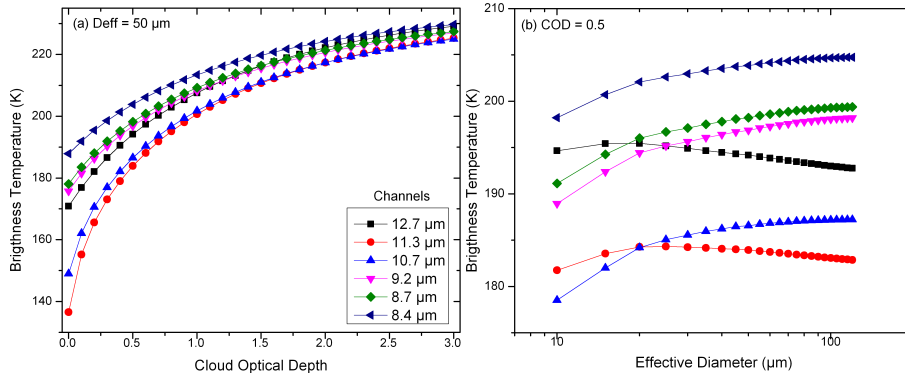


Figure 3. Variation in brightness temperature (T_b) with (a) cloud optical depth (COD) and (b) effective diameter (D_{eff}) for the six bands of the CIMEL CE-312. The color legend of the left hand graph applies to both graphs. The MODTRAN input parameters for this reference case are detailed in Table 2.

the response plateaus to variations of $\approx 1K$ or less. For the 11.3 and 12.7 μm channels, the responses are non monotonic (or considerably less monotonic) for the smaller values of D_{eff} and smoothly decrease with increasing D_{eff} beyond a peak in the 10 - 20 μm range. This decrease is associated with the relatively large spectral changes seen in the refractive index of ice particles at these larger wavelengths (see for example Warren and Brandt, 2008).

- As discussed above, IR radiance measurements are sensitive to a variety of cloud parameters as well as to the cloud environment. The simulation results in Figure 4 detail the band dependent effects of six different parameters by comparing changes in T_b induced by each parameter individually. **These were obtained for 1000 appropriately normalized samples of a random number generator with a normal probability distribution whose mean and standard deviation was controlled by the six parameter**

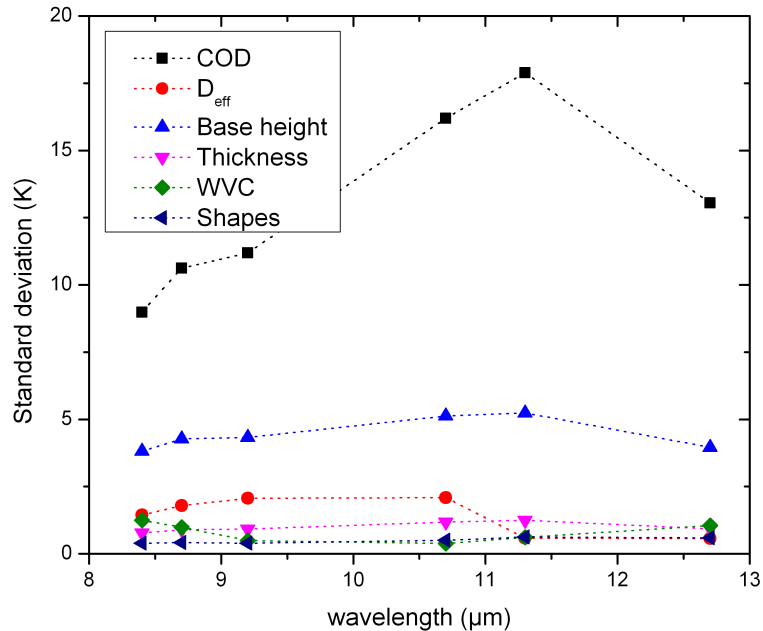


Figure 4. Sensitivity of T_b as a function of six key radiative transfer parameters. The standard deviations (in units of K) are obtained by stochastically varying, with a sample size of 1000, the parameters of interest within the limits given in the Table 2.

values of Table 2 (COD, D_{eff} , cloud base height, cloud thickness, column integrated water vapor of the atmosphere (WVC) and particle shape). The particle shape parameter is based on three particle characterizations as defined by Baum et al. (2014): severely roughened solid columns, a general habit mixture involving a set of 9 habits, and severely roughened aggregate of solid columns. The standard deviations in T_b that result from the variation of the six parameters are computed relative to the reference case defined above (Table 2). We note that there was little sensitivity to the choice of a 50 μm effective diameter for the reference case: changing this typical TIC2 value to a value more representative of TIC1 particles produced differences of less than 1 K in Figure 4.

Figure 4 shows that the chosen COD variation had the strongest T_b influence of all of the parameters, especially for the bands at 10.7 and 11.3 μm (as one could infer by referring to Figure 3a). Changes in D_{eff} (in red) lead to a standard deviation around 2 K for the four first bands as can be qualitatively appreciated by referring to Figure 3b. Changes in the altitude of the cloud induce a standard deviation up to 5 K. Indeed, because measurements of thermal IR radiometry are sensitive to temperature, a change in altitude causes a T_b difference that is sensitive to the range of temperatures within which the cloud is located. Cloud thickness and WVC are marginally important parameters in terms of the magnitude of the changes induced in T_b . If the altitude and the thickness of the clouds are known from vertical lidar (and radar) profiles then the magnitude of the altitude and cloud thickness uncertainties of Figure 4 will fall to levels commensurate with the standard deviations ascribed to the uncertainty in the ice particle shape (≈ 1 K as per the dark blue curve). This latter uncertainty (determined from the habit parameterizations listed in Table 2) is largely inflexible inasmuch as our ability to distinguish ice particle shape from lidar depolarization data

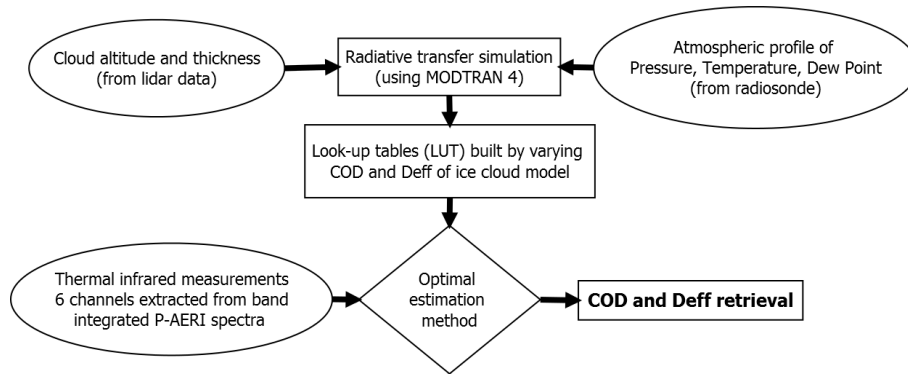


Figure 5. Flowchart of the retrieval method.

is extremely limited. Water vapor content (WVC) in the atmosphere, which remains relatively low during the polar winter at Eureka, has a weak absorption influence on the radiance measurements acquired in the CE-312 bands. Its associated uncertainty is commensurate with the uncertainties due to particle shape and cloud thickness: however integrated WVC is estimated from radiosonde profiles at Eureka and thus its uncertainty can be reduced to levels significantly below the particle shape and cloud thickness uncertainties. These reductions in the uncertainty of nominally known input parameters will be such that the variability of the parameters to be inverted (COD and D_{eff}) is significantly larger than the uncertainty of the known input parameters (for all bands in the case of the COD and at least in the case of the first 4 bands for D_{eff}).

5 Methodology

Our LIRAD objective was performed using LUTs and MODTRAN 4 radiative transfer simulations to parameterize the behavior of the downwelling zenith sky radiance as a function of key input parameters, including COD and D_{eff} . The methodology is represented in the flowchart of Figure 5. The core of this method, inspired by ground-based retrievals (e.g. Turner, 2005), is to compare thermal IR radiance measurements with LUTs derived from MODTRAN 4 simulations. This inverse problem is solved using the optimal estimation method (OEM) (Rodgers, 2000). The method seeks the state of maximal probability, conditional on the value of the measurements, associated errors and a priori knowledge. This OEM is an efficient inversion method that has already been employed for ice cloud retrievals (see for example Sourdeval et al., 2013).

The steps of the retrieval method are as follows:

1. First, knowledge of the cloud environment at the time of a given radiometer measurement is required. Specific input auxiliary data includes pressure, temperature and water vapor profiles from radiosonde data and the effective cloud-layer height from lidar backscatter data. The radiosonde parameters are interpolated to the radiometer times while the time of the selected lidar profile is the nearest to the radiometer time. To avoid the issue of interpolating radiosondes over extensively long periods of time, the cases were selected as close as possible to radiosonde launch times. Radiosonde humidity sensors are known to be subject to dry bias especially in dry conditions and could yield relative humidity

underestimates of 10 % (Rowe et al., 2008). The 6 channels are however far less sensitive to WVC than to COD (see Figure 4) and therefore the bias is expected to be lower in cloudy conditions. Cloud heights are estimated for sustained cloud features where clouds are defined by lidar backscatter coefficients greater than $1.10^{-6} \text{ m}^{-1} \cdot \text{sr}^{-1}$ and a lidar depolarization ratio greater than 20 % (thresholds were inspired by Shupe (2007) but adapted to a different vertical resolution of our lidar). Upper and lower cloud boundaries are then obtained where 4 continuous vertical samples of the lidar profile ($4 \times 30 = 120 \text{ m}$ for an AHSRL resolution of 30 m) comply with that requirement (preceded by a series of lower, non-cloud, samples).

2. Using MODTRAN 4, we simulated surface based zenith-looking brightness temperatures of a cloudy atmosphere as a function of the environmental data. A LUT is then constructed for 23 values of D_{eff} between 10 and 120 μm and 31 values of COD (from 0 to 3 with an increment of 0.1). Because T_b is so strongly dependent on COD, the LUT is linearly interpolated between MODTRAN 4 calculations with a COD increment of 0.01.
3. Brightness temperatures are then derived from radiance measurements in the six CIMEL CE-312 radiometer channels extracted from band integrated P-AERI spectra.
4. The OEM was used to compare the LUT spectra with the measured T_b spectra. This method requires precise quantification of errors attributed to each variable of the state and measurement vectors (as detailed in Rodgers, 2000, and in Appendix A). We retrieve the best estimates of COD and D_{eff} from the most optimal fit to the measured T_b .

Specific validation elements for our retrieval algorithm included profiles of the effective ice particle diameter prime (D'_{eff}) that were extracted from the combination of AHSRL and MMCR backscatter coefficients. This was carried out as per the technique developed by Donovan and van Lammeren (2001) and applied to the instruments at our study site (Eloranta et al., 2007). D'_{eff} is given by:

$$D'_{eff} = \sqrt[4]{\frac{\beta_{radar}}{\beta_{lidar}}} \quad (3)$$

where β_{radar} and β_{lidar} are the extinction cross-sections of the radar and lidar respectively. D'_{eff} can be related to D_{eff} assuming an analytical form for the size distribution which in our case was taken as a modified gamma distribution of hexagonal columns (Eloranta et al., 2007). In order to compare D_{eff} with our retrievals, we averaged this parameter over the vertical extent of a given cloud. We chose, for simplicity's sake, to assume a specific particle shape (i.e. the hexagonal column shape) when retrieving D_{eff} from the lidar/radar profiles to enable consistent comparisons with our passive retrievals. As a general quality assurance step for the radar data, those cases for which the radar backscatter coefficient was less than $10^{-15} \text{ m}^{-1} \cdot \text{sr}^{-1}$ (an empirically determined value of minimum detectability) were eliminated from any retrieval processing (this generally meant the elimination of TIC1 points). It is also important to state that radar signal is proportional to the sixth power of the hydrometeor diameter, whereas IR instruments are sensitive to the ratio of the third to the second moment. This means that the equivalent D_{eff} is not strictly the same and their comparison can generate biases in some conditions (see discussion in Turner, 2005).

The CODs from the passive algorithm was validated by comparison with estimates of COD derived from AHSRL observations using equation (4) and averaged over the cloud geometric thickness. By its design, the AHSRL measures two signals which can be processed to yield separate lidar returns for aerosol and molecular scattering, and then to make reliable measurements of the extinction profile. The optical depth τ across a range interval (r, r_0) is computed as:

$$5 \quad \tau(r) - \tau(r_0) = \frac{1}{2} \ln \left(\frac{\rho(r)}{\rho(r_0)} \right) - \frac{1}{2} \ln \left(\frac{S_m(r)}{S_m(r_0)} \right) \quad (4)$$

where ρ is the molecular density, and S_m is the range-squared, background corrected, molecular lidar return of the AHSRL. COD was calculated, using equation (4), across the cloud layer where the vertical cloud boundaries were determined according to the backscatter coefficient and depolarization criteria described above. Due to the very small angular field-of-view of the AHSRL receiver (45 μ rad), it is common to assume that the backscatter return is negligibly affected by multiple scattered photons (Eloranta et al., 2007). However, to better quantify the effect of multiple scattering, we applied Eloranta's (1998) approximate model to calculate the multiply scattered lidar returns for the 150 cloud cases. The inputs included molecular and particulate backscatter coefficients, effective diameters (inferred from the AHSRL+MMCR technique discussed below) and cloud height boundaries. The approximate model was employed to compute multiple scattering returns up to the 4th order. The impact of multiple scattering (MS) can then be evaluated in terms of COD inasmuch as multiple scattering lowers the apparent COD. From Equation (4), we define ΔCOD_{ms} as:

$$15 \quad \Delta COD_{ms} = -0.5 \log(1.0 + Pt/P1) \quad (5)$$

where Pt is an output of the MS model, representing all orders of multiple scattering while $P1$ is the single scattering return. This term can be used to correct the retrieved optical depth by inserting a multiplicative factor η , as per Platt (1973) to correct for the reduction of the extinction coefficient. The parameter η is not constant (Bissonnette, 2005) and Platt argued that it should vary between 0.5 and 1. Our best estimate of η over the ensemble of test cases was 0.95. This factor was used to correct the lidar-derived CODs that we employed for validation purposes in this manuscript.

Although intervals of P-AERI spectra (wavelength range of 3 - 20 μ m) were used to simulate the response of the CIMEL radiometer bands, the P-AERI instrument has more extensive capabilities and is sensitive to a larger range of D_{eff} , according to the absorption efficiency spectra (see Figure 2 in this article or Figure 5 in Yang et al., 2003). The mixed-phase cloud retrieval algorithm (MIXCRA) (Turner, 2005) is designed to estimate microphysical properties of both the ice and liquid components of a cloud using spectral IR radiances supplemented with data from various instruments. By using the spectral behavior of several "microwindows" between gaseous absorption lines in the thermal and far IR, MIXCRA can determine cloud phase and retrieve COD and D_{eff} (a detailed description of the algorithm can be found in Turner (2005)). Turner and Eloranta (2008) have demonstrated good agreement between the MIXCRA retrievals and HSRL optical depth measurements during an experiment at the ARM NSA site. Cox et al. (2014) describe the specifics of the Eureka implementation, including the auxiliary measurements that were employed (notably the AHSRL, MMCR, radiosonde data and a microwave radiometer). Within the scope of this current study, the cloud-phase determination from MIXCRA is used to ensure the comparison of ice-only cloud properties (i.e. those MIXCRA retrievals that yielded negligible liquid water path, LWP < 0.2 g.m⁻², were taken as being pure ice-cloud cases). MIXCRA results are used here as an alternative point of reference for our retrievals.

6 Results and Discussion

6.1 Physical Coherence of a Specific Case Study

In this section we seek to illustrate the temporal variation of particle size and COD in a precipitating cloud and demonstrate that our retrieval gives physically coherent results for a specific case that was chosen to exercise both the COD and D_{eff} retrievals. Figure 6 shows the selected 2009 winter campaign case where we compare AHSRL backscatter coefficient, the MMCR backscatter coefficient profile, the D_{eff} profile (which, as pointed out above, is related to D'_{eff}) and the results of our inversion (Figures 6a, 6b, 6c and 6d respectively).

Radar reflectivity is commonly used to describe the reflection, scattering and diffraction effects of a target on the incident signal. Radar reflectivity, expressed in dBZ, is logarithmically proportional to the backscatter coefficient and is proportional to the sixth power of the hydrometeors diameter (Battan, 1973). However, to ensure a consistent approach within the context of D_{eff} retrieval, we chose to display β_{radar} in Figure 6b.

One can see (Fig. 6d) that D_{eff} , for the lidar-radar technique (in blue), increases from 44 μm to 103 μm . This increase appears, in turn, to be correlated with cloud precipitation as evidenced by the accompanying decrease in altitude of the cloud structure seen in the lidar and radar profiles as well as increasing values of the radar Doppler fall velocity profiles (not shown). The passive D_{eff} retrievals (the green colored curve of Figure 6d) show a roughly similar trend from 20:00 to 23:00 (largely characterized however, by significantly smaller D_{eff} values). The insensitivity of the latter retrieval to larger size particles during the period from about 19:00 to 22:30 and the sudden jump in retrieved D_{eff} value after that time is the result of the type of asymptotic ceiling that one sees in Figure 3b and the choices made in the LUT algorithm retrieval: as one approaches the asymptotic ceiling from smaller D_{eff} values, there is clearly a progressive increase in the range of acceptable D_{eff} values for a given ΔT_b (a decrease in the robustness of the retrieved value). This example also illustrates an important issue related to our TIC1/TIC2 classification goal, where some points, around 20:00 appear to be classified as TIC1 particles by our algorithm while the lidar-radar values between 60 and 80 μm would be classified as TIC2 particles. One possible explanation is that the cloud vertical inhomogeneity, as evident in the cloud structure observable in Fig. 6a is the source of the misclassification. The regions of the effective diameter that are not detected by the lidar-radar retrieval (see the profiles of Fig. 6c) are indeed optically thick regions having more impact on the radiometric retrieval of Fig. 6d and that likely contain smaller particles.

The COD retrievals are, as one would expect, visually coherent with the general strength and extent of the lidar backscatter coefficient. After 2300 UTC our COD retrievals approach the limit of retrieval sensitivity suggested in Figure 3. This is manifested by an artificial non-monotonic increase in the variability of the retrieved COD (not very obvious in Figure 6 but obvious from our inversions in general) and is coherent with the asymptotic invariance of T_b with increasing COD in Figure 3. This example suggests that the dynamic evolution of cloud particle properties provided by continuous temporal analysis can lend support in helping to understand cloud dynamics and more specifically in discriminating TIC1 and TIC2 particles. In the latter case the passively retrieved evidence for progressively increasing values of COD and D_{eff} , supported by the lidar and

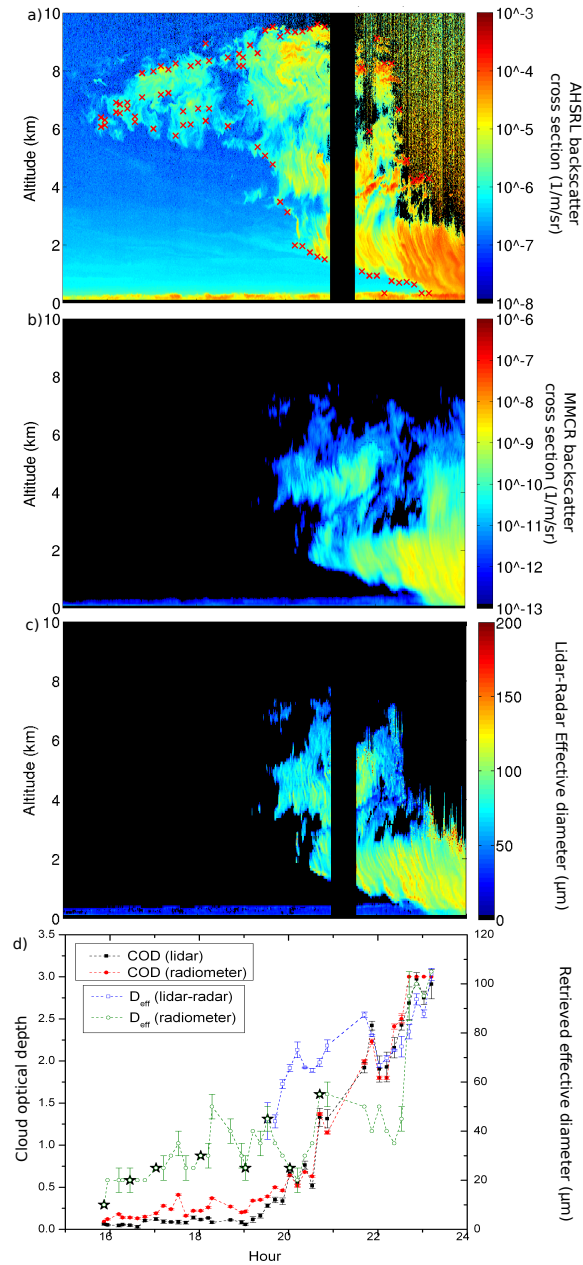


Figure 6. Evolution of validation and retrieval cloud parameters during a particular precipitating cloud event (January 13th, 2009) at Eureka. The error bars of the bottommost graph represent the retrieval errors. The error for the lidar COD retrievals is sufficiently small to be obscured by the size of the symbols representing this component. The red crosses, in the uppermost plot, are the cloud boundary limits used as input to our method. **The points upon which a star has been superimposed satisfied the criteria defined at the beginning of section 6.2 and are thus an example of points accepted in the validation part of this article.**

Table 3. Confusion matrix of the TIC1/TIC2 classification compared to lidar-radar retrievals. The term "err. comm." stands for the error of commission.

		lidar-radar	
		TIC1 (nb: 50) ($D_{eff} \leq 30 \mu\text{m}$)	TIC2 (nb: 100) ($D_{eff} > 30 \mu\text{m}$)
nb of observation: 150			
radiometer	TIC1	39	15
	TIC2	11	85
Overall accuracy = 83%		err. comm. TIC1 = 22%	err. comm. TIC2 = 15%

radar data, would lend more confidence to a classification result which indicated the presence of TIC2 type particles during the latter part of the day.

6.2 Validation of Our Retrieval Algorithm

Figure 7 shows COD and D_{eff} comparisons between the radiometric retrievals and the combined AHSRL and MMCR retrievals for over 150 ice clouds observed between September 2006 and March 2009. The selection of the 150 cases was driven by different criteria: a requirement for monolayer clouds; a cloud thickness greater than 200 m (to equal or exceed the MOD-TRAN vertical layer thickness of 200 m); that the time difference between two samples be more than 30 minutes; that the clouds were non-precipitating; a subjective criterion of cloud homogeneity; a constraint whereby the evidence for cases of TIC1 only, TIC2 only or a combination of the two was determined by whether the cloud was detected by the lidar and the radar; a requirement that the cloud be semi-transparent (AHSRL optical depth < 3); a constraint that the IR signal in any band not be saturated; that the visible optical depth should be greater than 0.1 and that the visible optical depth across the first two kilometers (where diamond dust particles are very often present in winter) should be less than 0.1. As an illustration of the influence of these criteria, only 8 of the 41 points seen in Figure 6 were selected to be part of the 150 cases.

Those clouds are not meant to be representative of the Eureka cloud climatology. Their mean base altitude (5.2 km) and vertical extent (2.3 km) is substantially higher than a cloud climatology that was generated across four years of data (Shupe et al., 2011) (1.8 km and 2 km respectively) as well as the CALIPSO/CloudSat and ground-based climatologies on the vertical distribution of ice-only cloud (Blanchard et al., 2014).

The COD results (Figure 7a) show a significant correlation with lidar ($R^2 = 0.95$) over a large optical depth range (from 0.1 to 2.6). This level of agreement confirms the relatively strong sensitivity of the ensemble of the radiometer bands to the COD (c.f. Figure 3a). As seen in that figure, the T_b sensitivity decreases with increasing COD such that the asymptotic behavior of the COD variation tends towards an upper limit of COD detectability of 2-3 (where the spread of T_b values \approx the measured uncertainty in those T_b values).

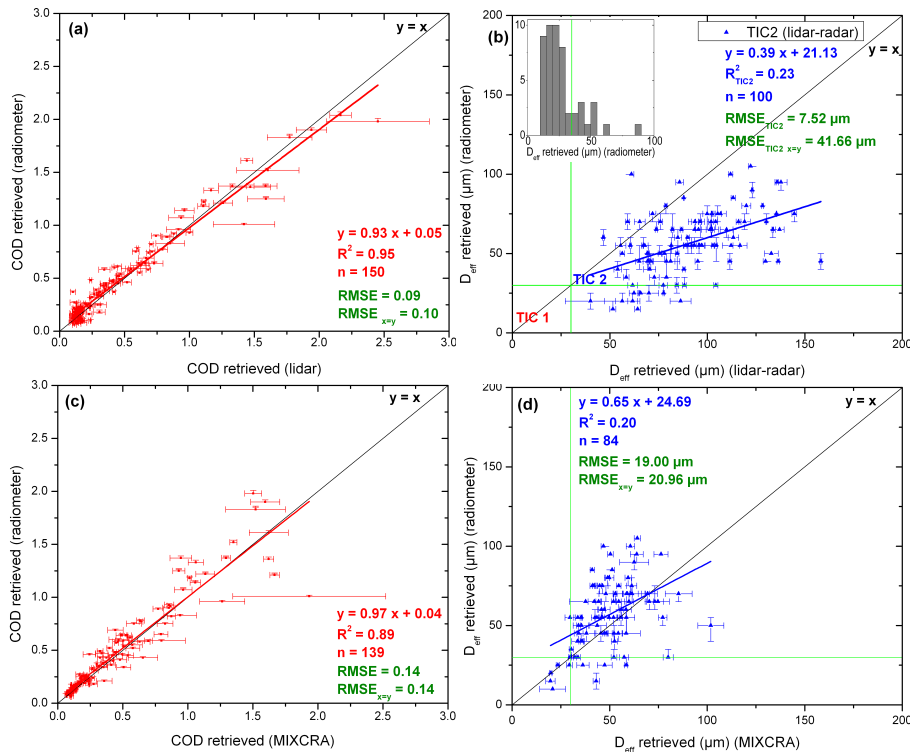


Figure 7. Radiometer-based retrieval results for (a) CODs compared with lidar derived CODs and (b) D_{eff} compared with the lidar-radar retrieval product. The same comparisons, with MIXCRA retrievals being the reference, are shown in graphs (c) and (d). TIC1 results, because of the lidar-radar insensitivity of these small particles, are excluded from the scattergram but their D_{eff} frequency distribution is shown in the inlaid histogram. The D_{eff} comparisons with the MIXCRA retrievals show fewer points than the comparisons with the lidar-radar retrieval because the MIXCRA retrievals of D_{eff} have relatively large uncertainties for cases where $COD \leq 0.2$ (and thus are not shown).

The quality of the particle size retrieval was difficult to quantify because the thermal IR channels become increasingly less sensitive to particles larger than $\approx 100 \mu\text{m}$ as suggested in Figure 2b. This insensitivity to large particle sizes likely contributes to the large dispersion (and hence the marginal correlation) of retrieved TIC2 values seen in Figure 7b. The separation between TIC1 and TIC2 particles was effected based on the D_{eff} values from the lidar-radar retrieval: the lower bound TIC2 value / upper bound TIC1 value was set at $30 \mu\text{m}$. We show below that while the radiometer D_{eff} retrievals are of significantly less amplitude than the lidar-radar retrievals, **the $30 \mu\text{m}$ crossover criterion from TIC1 to TIC2 is sufficiently well delineated to** achieve acceptable classification accuracy. One factor that complicated the D_{eff} comparison over all particles sizes was the MMCR sensitivity limit at smaller particle sizes ($\approx 30\text{-}40 \mu\text{m}$) and the constraints this imposed on the lidar-radar retrieval. For that reason, the TIC1 results were not considered in the R^2 statistics. However, the TIC1 frequency distribution derived for our retrieval algorithm (inlaid histogram in Figure 7b) confirms the robustness of the retrievals inasmuch as 78% of the retrieved TIC1 population have a D_{eff} less than $30 \mu\text{m}$ (and 96% less or equal to $50 \mu\text{m}$).

Table 4. Confusion matrix of the TIC1/TIC2 classification compared to MIXCRA retrievals. The term "err. comm." stands for the error of commission.

		MIXCRA	
		TIC1 (nb: 7) ($D_{eff} \leq 30 \mu\text{m}$)	TIC2 (nb: 77) ($D_{eff} > 30 \mu\text{m}$)
nb of observation: 84			
radiometer	TIC1	6	9
	TIC2	1	68
Overall accuracy = 88%		err. comm. TIC1 = 14%	err. comm. TIC2 = 12%

The lack of TIC1 sensitivity of the lidar-radar combination means that our radiometric retrieval algorithm cannot be verified with the lidar-radar retrieval in the TIC1 particle-size region. Nonetheless, the lidar-radar classification scheme of Section 3 can at least separate out TIC1 and TIC2 cases. Table 3 presents the retrieved results in terms of the TIC1/TIC2 classification compared with the validation data. A threshold value of $30 \mu\text{m}$ was used to discriminate between the two classes in the case of the radiometer retrieval. Those cases for which β_{radar} was less than $10^{-15} \text{ m}^{-1} \cdot \text{sr}^{-1}$ were classified as TIC1 cloud (this cutoff is illustrated by the dark regions of the β_{radar} plot seen in the case study of Figure 6). The classification yielded satisfactory results with an overall accuracy of 83%. The TIC1 retrievals were associated with a 22% detection (omission) error ($11/50 \times 100$) while the TIC2 omission error was 15%. We should note that the classification results are moderately sensitive to the threshold D_{eff} value assumed between the TIC1 and TIC2 classes: for threshold values of 35 and $40 \mu\text{m}$, the overall accuracies were respectively 82% and 82% with moderately smaller TIC1 omission errors (18% and 12% respectively).

A comparison with the MIXCRA retrievals (Figures 7c and 7d and Table 4) amounts to a coherency check between the two passive inversion techniques. While limited in terms of absolute validation, this comparison effectively reduces the array of confounding influences that can affect the retrieval quality of both approaches (and in so doing, permits a more direct evaluation of the strengths and weaknesses of either technique). In Figure 7c, the good correlation between MIXCRA's and our COD retrievals and a slope near 1 confirm the robustness of the COD retrieval. The good COD correlation is expected inasmuch as a similar degree of correlation between MIXCRA and AHSRL results for ice-only clouds was previously observed (Turner and Eloranta, 2008). The comparison of the D_{eff} values from our radiometer retrieval and the MIXCRA retrieval (Figure 7d) shows a somewhat better absolute agreement relative to the comparisons of our radiometer retrieval with the lidar-radar retrieval (point scatter closer to $y = x$ but a value of R^2 which is also at the margins of significance).

Figure 8 indicates that all of cases with $\text{COD} > 1$ were classified as TIC2 for the passive and active retrievals. Clouds classified as TIC1 are, in contrast, preferentially associated with COD less than 0.3. The degree of TIC1/TIC2 classification coherence between the lidar-radar and the radiometer retrievals, in the histogram of Figure 8, illustrates the value of our semi-qualitative (binary) classification approach for an application (the DGF effect of Blanchet and Girard, 1994) that specifically requires such

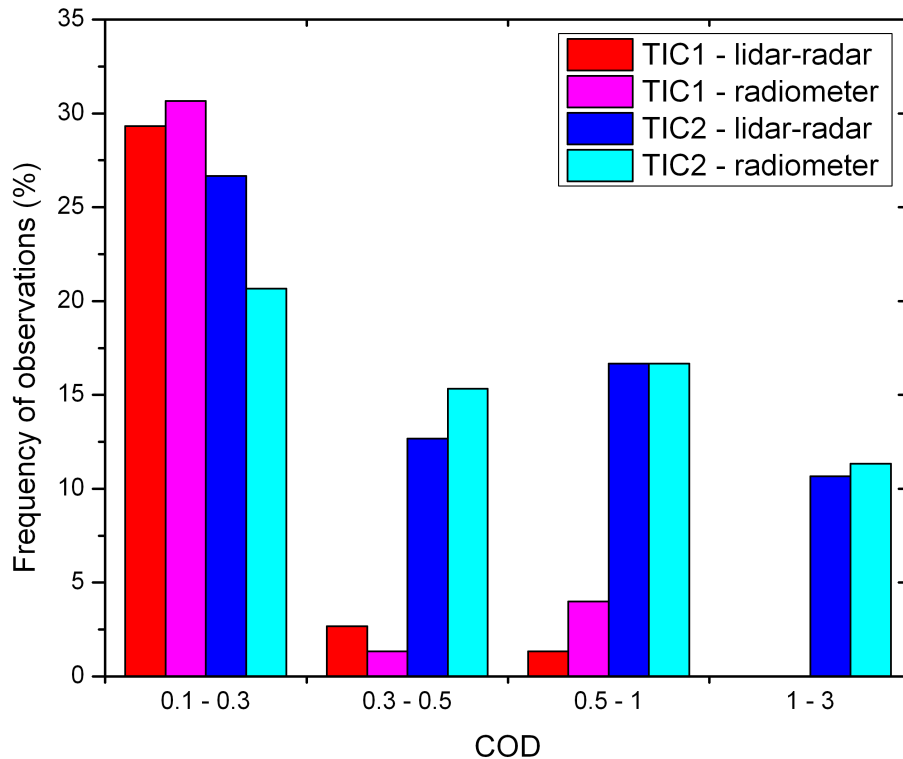


Figure 8. Histogram of active and passive classifications of TIC (TIC1 in red and pink; TIC2 in blue and cyan) as a function of COD.

binary information.

In order to better understand the physical implications of the retrievals, we plotted, in Figure 9, passive TIC1/TIC2 discrimination results along with downwelling longwave cloud radiative forcing (DLCRF). These data represent the 150 cloud cases that we employed above for the retrieval validation. The general distribution of the DLCRF is similar to the Figure 4 results of Cox et al. (2014) who applied the MIXCRA algorithm continuously (without the separation into specific events) during the same period. As DLCRF is closely linked to the COD, one can note that the TIC1 generally have a small DLCRF of less than $10 \text{ W}\cdot\text{m}^{-2}$. The DGF impact of the TIC2 particles (meaning their progressive removal by precipitation) would accordingly be that their radiative forcing influence would progressively decrease with an attendant cooling due to a reduction in thermal interaction with the remaining TIC1 particles (and the unprecipitated TIC2 particles). A long-term analysis would help to support modeling conclusions on the impact of acid-coated ice nuclei on Arctic cloud as reported by Girard et al. (2013). These authors reported a mean downward longwave (negative) radiation anomaly at the surface of $-3 -5 \text{ W}/\text{m}^2$, close to Eureka.

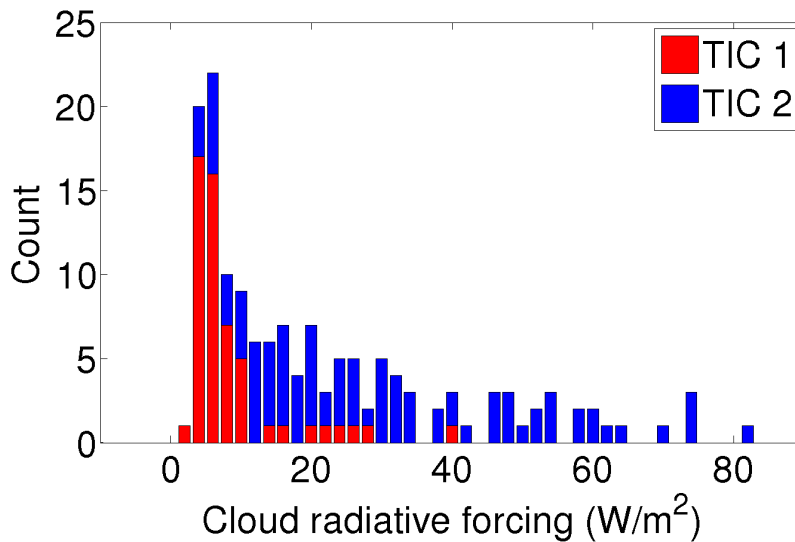


Figure 9. Downwelling longwave cloud radiative forcing of the 150 cases decomposed in TIC1 and TIC2

6.3 Additional Sensitivity Studies

The effect of particle shape on the retrievals was analyzed by re-applying the retrieval algorithm to the 150 thin ice clouds using particle shapes other than our solid column crystal standard (not shown). Retrievals results showed that the shape employed in the LUT generation has only a small influence in the performance of our retrievals (as one could have inferred from Figure 4).

- 5 This confirms the previous conclusion from Wendisch et al. (2007). The validation of COD retrievals, expressed in terms of RMSE, varied from 0.10 to 0.11 as a function of shape while overall classification accuracy varied from 82% to 83% (versus the results of 0.10 and 83% respectively for the solid column crystal shape).

10 We exploited the extinction coefficient profile retrieval obtainable from equation (4) in order to evaluate the impact of the extinction profile as an added dimension of input to the radiative transfer model. Rather than assuming a constant extinction coefficient profile across the width of the cloud, we broke the cloud into vertical segments and obtained a coarse vertical profile. Retrieval results showed a moderate impact of the extinction profile since the RMSE is 0.09 instead of 0.10 while the overall classification accuracy remained at 83%. A similar comparison from MIXCRA results (not shown here) confirms the moderate impact of the use of real extinction profiles.

15 7 Conclusions

We developed a simple inversion technique to retrieve the optical depth and effective particulate diameter of Arctic thin ice clouds from a multi-broadband thermal radiometer using lidar and radiosonde measurements as auxiliary inputs to the inversion

routine. Specific validation elements were extracted from the combination of lidar and radar data, as well as AERI data. Our retrieval technique was applied to 150 thin ice clouds measured at the PEARL observatory (Nunavut, Canada).

The results of this study demonstrate the potential for retrieving key ice cloud parameters from thermal IR radiometry (with bands between 8 and 13 μm). The COD retrieval algorithm showed good agreement with the validation COD obtained from integrated lidar profiles. The retrievals of D_{eff} showed marginal correlation for particle sizes restricted to the TIC2 category (a constraint that was driven by the insensitivity of the lidar-radar retrievals to small cloud particles). This is likely due to the weak sensitivity of thermal IR measurements for particles larger than $\approx 100 \mu\text{m}$. However, a classification of thin ice clouds in terms of TIC1 and TIC2 classes, using a threshold discrimination of 30 μm results in a significant classification accuracy of 83% for our passive retrieval algorithm. Further analysis showed that the extinction profile and particle shape had relatively weak impact on the retrieval results. Comparisons with the MIXCRA algorithm confirm the robustness of the optical depth retrieval.

An important application of our work would be to deploy this technique as part of a network of low-cost and robust instruments to monitor Arctic clouds. Because their occurrence, type and altitude are spatially inhomogeneous (according to Eastman and Warren, 2010; Shupe et al., 2011), we believe that additional ground-based stations would be helpful to broaden our knowledge of arctic ice clouds. Aside from being a ground-based retrieval approach in its own right (in tandem with a lidar system), this method can also be used for comparison with CALIPSO's level 2 products. The CALIPSO remote sensing suite technique employs an onboard imaging IR radiometer and the CALIOP lidar to enable the retrieval of particle size and optical depth across a narrow swath image (Garnier et al., 2012). Our retrieval, viewed as a CALIPSO validation technique is rendered all the more interesting because of the geographic position of the PEARL site; it is a high-Arctic site that sees frequent thin-cloud events and its position near the maximum latitude of the CALIOP polar orbit ensures that there are frequent overpasses of that sensor package (within a radius of hundreds of km).

Appendix A: Optimal estimation method

The optimal estimation method (OEM, Rodgers, 2000) is an efficient solution to inverse problems, especially in atmospheric science. A good understanding of the technique and its associated errors is a prerequisite for the proper use of this method. Inasmuch as our application of OEM is very similar to Sourdeval's (Sourdeval et al., 2013), we used the same formalism to define the OEM components. As set out in Section 5, the OEM goal is to retrieve state variables having the maximum probability of occurrence by minimizing a cost function ϕ :

$$\phi = (y - F(x))^T S_e^{-1} (y - F(x)) + (x - x_a)^T S_a^{-1} (x - x_a) \quad (\text{A1})$$

where F is the forward model, i.e. radiative transfer computation in our case. The state (x), a priori (x_a) and measurement (y) vectors are defined as:

$$x = \begin{pmatrix} D_{eff} \\ COD \end{pmatrix}; x_a = \begin{pmatrix} D_{eff-a} \\ COD_a \end{pmatrix}; y = \begin{pmatrix} T_{b_8.4} \\ T_{b_8.7} \\ T_{b_9.2} \\ T_{b_10.7} \\ T_{b_11.3} \\ T_{b_12.7} \end{pmatrix} \quad (A2)$$

The a priori vector is the prior knowledge of the state vector, and typically corresponds to climatological values of the state vector components. **In our case, the reference case of Table 2 was used to define the a priori vector and its covariance matrix.** Even if any particular a priori vector values have an impact on the retrievals, it is common to attribute large uncertainties to them in the covariance matrix S_a in order to let the measurement vector be the dominant driver of the retrieval. This covariance matrix is given by:

$$S_a = \begin{pmatrix} \sigma_{D_{eff-a}}^2 & 0 \\ 0 & \sigma_{COD_a}^2 \end{pmatrix} \quad (A3)$$

The total error covariance matrix S_e is the quadratic sum of the measurement error covariance matrix S_y and the forward model parameter uncertainty covariance matrix S_f . We assumed that the components of the measurement or state vectors are independent (i.e., that the covariance matrix is diagonal). **The measurement errors depend on the accuracy of the radiometer (which is assumed to be 0.1 K for each band, Brogniez et al., 2003). We presumed the measurement errors are wavelength-independent.** The forward model errors represent the quadrature sum of the uncertainties of each input parameter (cloud base height, thickness, water vapor content and particle size) of the MODTRAN calculation. **We then use the sensitivity study, Figure 4, to define the standard error ($\sigma/\sqrt{1000}$) of each parameter from the stochastic analysis. The components of S_e are close to 0.30 K (between 0.28 and 0.34 K) and of the same order of magnitude as S_y .**

Acknowledgements. We would like to thank the Canadian Network for the Detection of Atmospheric Change (CANDAC), Study of Environmental Arctic Change (SEARCH) and **Environment and Climate Change Canada** for their operational support. We are grateful to Von Walden, of the Washington State University, for the quality checked P-AERI data. This research was supported by the Natural Sciences and Engineering Research Council of Canada (NSERC), Fonds Québécois de la Recherche sur la Nature et les Technologies (FQRNT) and the Canadian Space Agency (CSA). This work was also partially supported by the U.S. Department of Energy Atmospheric System Research Program DE-SC0008830.

References

- Allen, J. R.: Measurements of Cloud Emissivity in the 8-13 μ Waveband, *J. Appl. Meteor.*, 10, 260–265, doi:10.1175/1520-0450(1971)010<0260:MOCEIT>2.0.CO;2, [http://dx.doi.org/10.1175/1520-0450\(1971\)010<0260:MOCEIT>2.0.CO;2](http://dx.doi.org/10.1175/1520-0450(1971)010<0260:MOCEIT>2.0.CO;2), 1971.
- Baran, A. J.: From the single-scattering properties of ice crystals to climate prediction: A way forward, *Atmospheric Research*, 112, 45 – 69, doi:<http://dx.doi.org/10.1016/j.atmosres.2012.04.010>, <http://www.sciencedirect.com/science/article/pii/S0169809512001160>, 2012.
- 5 Battan, L. J.: Radar observation of the atmosphere. (The University of Chicago Press) 1973. PP X, 324; 125 figures, 21 tables., *Quarterly Journal of the Royal Meteorological Society*, 99, 793–793, doi:10.1002/qj.49709942229, <http://dx.doi.org/10.1002/qj.49709942229>, 1973.
- Baum, B. A., Yang, P., Heymsfield, A. J., Bansemmer, A., Cole, B. H., Merrelli, A., Schmitt, C., and Wang, C.: Ice cloud single-scattering property models with the full phase matrix at wavelengths from 0.2 to 100 μ m, *Journal of Quantitative Spectroscopy and Radiative Transfer*, 10 146, 123 – 139, doi:<http://dx.doi.org/10.1016/j.jqsrt.2014.02.029>, <http://www.sciencedirect.com/science/article/pii/S0022407314000867>, electromagnetic and Light Scattering by Nonspherical Particles {XIV}, 2014.
- Berk, A., Anderson, G. P., Acharya, P. K., Chetwynd, J. H., Bernstein, L. S., Shettle, E. P., Matthew, M. W., and Adler-Golden, S. M.: *Modtran 4 user's manual*, Air Force Research Laboratory, 1999.
- Bissonnette, L. R.: Lidar: Range-Resolved Optical Remote Sensing of the Atmosphere, chap. Lidar and Multiple Scattering, Klaus Weitkamp 15 editor, *Springer Series in Optical Sciences*, Springer-Verlag, New York, 2005.
- Blanchard, Y., Pelon, J., Eloranta, E. W., Moran, K. P., Delanoë, J., and Sèze, G.: A Synergistic Analysis of Cloud Cover and Vertical Distribution from A-Train and Ground-Based Sensors over the High Arctic Station Eureka from 2006 to 2010, *Journal of Applied Meteorology and Climatology*, 53, 2553–2570, doi:10.1175/JAMC-D-14-0021.1, <http://dx.doi.org/10.1175/JAMC-D-14-0021.1>, 2014.
- Blanchet, J.-P. and Girard, E.: Arctic /'greenhouse effect/', *Nature*, 371, 383–383, <http://dx.doi.org/10.1038/371383a0>, 1994.
- 20 Blanchet, J.-P., Royer, A., Châteauneuf, F., Bouzid, Y., Blanchard, Y., Hamel, J.-F., de Lafontaine, J., Gauthier, P., O'Neill, N. T., Pancrati, O., and Garand, L.: TICFIRE: a far infrared payload to monitor the evolution of thin ice clouds, doi:10.1117/12.898577, <http://dx.doi.org/10.1117/12.898577>, 2011.
- Bourdages, L., Duck, T. J., Lesins, G., Drummond, J. R., and Eloranta, E. W.: Physical properties of High Arctic tropospheric particles during winter, *Atmospheric Chemistry and Physics*, 9, 6881–6897, doi:10.5194/acp-9-6881-2009, [http://www.atmos-chem-phys.net/9/](http://www.atmos-chem-phys.net/9/6881/2009/) 25 [6881/2009/](http://www.atmos-chem-phys.net/9/6881/2009/), 2009.
- Brognez, G., Pietras, C., Legrand, M., Dubuisson, P., and Haeffelin, M.: A High-Accuracy Multiwavelength Radiometer for In Situ Measurements in the Thermal Infrared. Part II: Behavior in Field Experiments, *Journal of Atmospheric and Oceanic Technology*, 20, 1023–1033, doi:10.1175/1520-0426(2003)20<1023:AHMRFI>2.0.CO;2, [http://dx.doi.org/10.1175/1520-0426\(2003\)20<1023:AHMRFI>2.0.CO;2](http://dx.doi.org/10.1175/1520-0426(2003)20<1023:AHMRFI>2.0.CO;2), 2003.
- 30 Brogniez, G., Parol, F., Becu, L., Pelon, J., Jourdan, O., Gayet, J.-F., Auriol, F., Verwaerde, C., Balois, J.-Y., and Damiri, B.: Determination of cirrus radiative parameters from combination between active and passive remote sensing measurements during FRENCH/DIRAC 2001, *Atmospheric Research*, 72, 425–452, doi:10.1016/j.atmosres.2004.03.026, <http://www.sciencedirect.com/science/article/pii/S016980950400081X>, 2004.
- Chiriaco, M., Chepfer, H., Noel, V., Delaval, A., Haeffelin, M., Dubuisson, P., and Yang, P.: Improving Retrievals of Cirrus Cloud Particle Size Coupling Lidar and Three-Channel Radiometric Techniques, *Mon. Wea. Rev.*, 132, 1684–1700, doi:10.1175/1520-0493(2004)132<1684:IROCCP>2.0.CO;2, [http://dx.doi.org/10.1175/1520-0493\(2004\)132<1684:IROCCP>2.0.CO;2](http://dx.doi.org/10.1175/1520-0493(2004)132<1684:IROCCP>2.0.CO;2), 2004.

- Comstock, J. M. and Sassen, K.: Retrieval of Cirrus Cloud Radiative and Backscattering Properties Using Combined Lidar and Infrared Radiometer (LIRAD) Measurements, *Journal of Atmospheric and Oceanic Technology*, 18, 1658–1673, doi:10.1175/1520-0426(2001)018<1658:ROCCRA>2.0.CO;2, [http://dx.doi.org/10.1175/1520-0426\(2001\)018<1658:ROCCRA>2.0.CO;2](http://dx.doi.org/10.1175/1520-0426(2001)018<1658:ROCCRA>2.0.CO;2), 2001.
- 5 Cox, C. J., Turner, D. D., Rowe, P. M., Shupe, M. D., and Walden, V. P.: Cloud Microphysical Properties Retrieved from Downwelling Infrared Radiance Measurements Made at Eureka, Nunavut, Canada (2006–09), *J. Appl. Meteor. Climatol.*, 53, 772–791, doi:10.1175/JAMC-D-13-0113.1, <http://dx.doi.org/10.1175/JAMC-D-13-0113.1>, 2014.
- Delamere, J. S., Clough, S. A., Payne, V. H., Mlawer, E. J., Turner, D. D., and Gamache, R. R.: A far-infrared radiative closure study in the Arctic: Application to water vapor, *Journal of Geophysical Research: Atmospheres*, 115, n/a–n/a, doi:10.1029/2009JD012968, <http://dx.doi.org/10.1029/2009JD012968>, 2010.
- 10 Donovan, D. P. and van Lammeren, A. C. A. P.: Cloud effective particle size and water content profile retrievals using combined lidar and radar observations 1. Theory and examples, *J. Geophys. Res.*, 106, 27 425–27 448, <http://dx.doi.org/10.1029/2001JD900243>, 2001.
- Dubuisson, P., Giraud, V., Pelon, J., Cadet, B., and Yang, P.: Sensitivity of Thermal Infrared Radiation at the Top of the Atmosphere and the Surface to Ice Cloud Microphysics, *J. Appl. Meteor. Climatol.*, 47, 2545–2560, doi:10.1175/2008JAMC1805.1, <http://dx.doi.org/10.1175/2008JAMC1805.1>, 2008.
- 15 Eastman, R. and Warren, S.: Arctic Cloud Changes from Surface and Satellite Observations, *Journal of Climate*, 23, 4233–4242, doi:10.1175/2010JCLI3544.1, <http://dx.doi.org/10.1175/2010JCLI3544.1>, 2010.
- Ebert, E. E. and Curry, J. A.: A Parameterization of Ice Cloud Optical Properties for Climate Models, *J. Geophys. Res.*, 97, 3831–3836, <http://dx.doi.org/10.1029/91JD02472>, 1992.
- Eloranta, E. W.: Lidar: Range-Resolved Optical Remote Sensing of the Atmosphere, chap. High Spectral Resolution Lidar, Klaus Weitkamp editor, *Springer Series in Optical Sciences*, Springer-Verlag, New York, 2005.
- 20 Eloranta, E. W., Uttal, T., and Shupe, M.: Cloud particle size measurements in Arctic clouds using lidar and radar data, in: 2007 IEEE International Geoscience and Remote Sensing Symposium, pp. 2265–2267, doi:10.1109/IGARSS.2007.4423292, 2007.
- Feingold, G. and McComiskey, A.: ARM’s Aerosol-Cloud-Precipitation Research (Aerosol Indirect Effects), *Meteorological Monographs*, 57, 22.1–22.15, doi:10.1175/AMSMONOGRAPHIS-D-15-0022.1, <http://dx.doi.org/10.1175/AMSMONOGRAPHIS-D-15-0022.1>, 2016.
- 25 Garnier, A., Pelon, J., Dubuisson, P., Faivre, M., Chomette, O., Pascal, N., and Kratz, D. P.: Retrieval of Cloud Properties Using CALIPSO Imaging Infrared Radiometer. Part I: Effective Emissivity and Optical Depth, *Journal of Applied Meteorology and Climatology*, 51, 1407–1425, doi:10.1175/JAMC-D-11-0220.1, <http://dx.doi.org/10.1175/JAMC-D-11-0220.1>, 2012.
- Girard, E., Dueymes, G., Du, P., and Bertram, A. K.: Assessment of the effects of acid-coated ice nuclei on the Arctic cloud microstructure, atmospheric dehydration, radiation and temperature during winter, *International Journal of Climatology*, 33, 599–614, doi:10.1002/joc.3454, <http://dx.doi.org/10.1002/joc.3454>, 2013.
- 30 Grenier, P., Blanchet, J.-P., and Muñoz-Alpizar, R.: Study of polar thin ice clouds and aerosols seen by CloudSat and CALIPSO during midwinter 2007, *Journal of Geophysical Research: Atmospheres*, 114, n/a–n/a, doi:10.1029/2008JD010927, <http://dx.doi.org/10.1029/2008JD010927>, 2009.
- Hansen, J. E. and Travis, L. D.: Light scattering in planetary atmospheres, *Space Science Reviews*, 16, 527–610, <http://dx.doi.org/10.1007/BF00168069>, 10.1007/BF00168069, 1974.
- 35 Heymsfield, A. J., Krämer, M., Luebke, A., Brown, P., Cziczo, D. J., Franklin, C., Lawson, P., Lohmann, U., McFarquhar, G., Ulanowski, Z., and Tricht, K. V.: Cirrus Clouds, *Meteorological Monographs*, 58, 2.1–2.26, doi:10.1175/AMSMONOGRAPHIS-D-16-0010.1, <http://dx.doi.org/10.1175/AMSMONOGRAPHIS-D-16-0010.1>, 2017.

- Illingworth, A. J., Barker, H. W., Beljaars, A., Ceccaldi, M., Chepfer, H., Clerbaux, N., Cole, J., Delanoë, J., Domenech, C., Donovan, D. P., Fukuda, S., Hiraoka, M., Hogan, R. J., Huenerbein, A., Kollias, P., Kubota, T., Nakajima, T., Nakajima, T. Y., Nishizawa, T., Ohno, Y., Okamoto, H., Oki, R., Sato, K., Satoh, M., Shephard, M. W., Velazquez-Blazquez, A., Wandinger, U., Wehr, T., and van Zadelhoff, G.-J.: The EarthCARE Satellite: The Next Step Forward in Global Measurements of Clouds, Aerosols, Precipitation, and Radiation, *Bulletin of the American Meteorological Society*, 96, 1311–1332, doi:10.1175/BAMS-D-12-00227.1, <http://dx.doi.org/10.1175/BAMS-D-12-00227.1>, 2015.
- Inoue, T.: On the temperature and effective emissivity determination of semi-transparent cirrus clouds by bi-spectral measurements in the 10 μ window region, *Journal of the Meteorological Society of Japan*, 63, 88–99, 1985.
- IPCC: Climate Change 2013: The Physical Science Basis. Contribution of Working Group I to the Fifth Assessment Report of the Intergovernmental Panel on Climate Change, Cambridge University Press, Cambridge, United Kingdom and New York, NY, USA, doi:10.1017/CBO9781107415324, www.climatechange2013.org, 2013.
- Jiang, J. H., Su, H., Zhai, C., Perun, V. S., Del Genio, A., Nazarenko, L. S., Donner, L. J., Horowitz, L., Seman, C., Cole, J., Gettelman, A., Ringer, M. A., Rotstayn, L., Jeffrey, S., Wu, T., Brient, F., Dufresne, J.-L., Kawai, H., Koshiro, T., Watanabe, M., LÉcuyer, T. S., Volodin, E. M., Iversen, T., Drange, H., Mesquita, M. D. S., Read, W. G., Waters, J. W., Tian, B., Teixeira, J., and Stephens, G. L.: Evaluation of cloud and water vapor simulations in CMIP5 climate models using NASA 'A-Train' satellite observations, *Journal of Geophysical Research: Atmospheres*, 117, n/a–n/a, doi:10.1029/2011JD017237, <http://dx.doi.org/10.1029/2011JD017237>, d14105, 2012.
- Jouan, C., Pelon, J., Girard, E., Ancellet, G., Blanchet, J. P., and Delanoë, J.: On the relationship between Arctic ice clouds and polluted air masses over the North Slope of Alaska in April 2008, *Atmospheric Chemistry and Physics*, 14, 1205–1224, doi:10.5194/acp-14-1205-2014, <http://www.atmos-chem-phys.net/14/1205/2014/>, 2014.
- Knuteson, R. O., Revercomb, H. E., Best, F. A., Ciganovich, N. C., Dedecker, R. G., Dirks, T. P., Ellington, S. C., Feltz, W. F., Garcia, R. K., Howell, H. B., Smith, W. L., Short, J. F., and Tobin, D. C.: Atmospheric Emitted Radiance Interferometer. Part I: Instrument Design, *Journal of Atmospheric and Oceanic Technology*, 21, 1763–1776, doi:10.1175/JTECH-1662.1, <http://dx.doi.org/10.1175/JTECH-1662.1>, 2004a.
- Knuteson, R. O., Revercomb, H. E., Best, F. A., Ciganovich, N. C., Dedecker, R. G., Dirks, T. P., Ellington, S. C., Feltz, W. F., Garcia, R. K., Howell, H. B., Smith, W. L., Short, J. F., and Tobin, D. C.: Atmospheric Emitted Radiance Interferometer. Part II: Instrument Performance, *Journal of Atmospheric and Oceanic Technology*, 21, 1777–1789, doi:10.1175/JTECH-1663.1, <http://dx.doi.org/10.1175/JTECH-1663.1>, 2004b.
- Legrand, M., Pietras, C., Brogniez, G., Haeffelin, M., Abuhassan, N. K., and Sicard, M.: A High-Accuracy Multiwavelength Radiometer for In Situ Measurements in the Thermal Infrared. Part I: Characterization of the Instrument, *Journal of Atmospheric and Oceanic Technology*, 17, 1203–1214, doi:10.1175/1520-0426(2000)017<1203:AHAMRF>2.0.CO;2, [http://dx.doi.org/10.1175/1520-0426\(2000\)017<1203:AHAMRF>2.0.CO;2](http://dx.doi.org/10.1175/1520-0426(2000)017<1203:AHAMRF>2.0.CO;2), 2000.
- Libois, Q., Proulx, C., Ivanescu, L., Coursol, L., Pelletier, L. S., Bouzid, Y., Barbero, F., Girard, E., and Blanchet, J.-P.: A microbolometer-based far infrared radiometer to study thin ice clouds in the Arctic, *Atmospheric Measurement Techniques*, 9, 1817–1832, doi:10.5194/amt-9-1817-2016, <http://www.atmos-meas-tech.net/9/1817/2016/>, 2016.
- Lubin, D.: Infrared Radiative Properties Of the Maritime Antarctic Atmosphere, *J. Climate*, 7, 121–140, doi:10.1175/1520-0442(1994)007<0121:IRPOTM>2.0.CO;2, [http://dx.doi.org/10.1175/1520-0442\(1994\)007<0121:IRPOTM>2.0.CO;2](http://dx.doi.org/10.1175/1520-0442(1994)007<0121:IRPOTM>2.0.CO;2), 1994.

- Mahesh, A., Walden, V. P., and Warren, S. G.: Ground-Based Infrared Remote Sensing of Cloud Properties over the Antarctic Plateau. Part II: Cloud Optical Depths and Particle Sizes, *J. Appl. Meteor.*, 40, 1279–1294, doi:10.1175/1520-0450(2001)040<1279:GBIRSO>2.0.CO;2, [http://dx.doi.org/10.1175/1520-0450\(2001\)040<1279:GBIRSO>2.0.CO;2](http://dx.doi.org/10.1175/1520-0450(2001)040<1279:GBIRSO>2.0.CO;2), 2001.
- Meador, W. E. and Weaver, W. R.: Two-Stream Approximations to Radiative Transfer in Planetary Atmospheres: A Unified Description of Existing Methods and a New Improvement, *Journal of the Atmospheric Sciences*, 37, 630–643, doi:10.1175/1520-0469(1980)037<0630:TSATRT>2.0.CO;2, [http://dx.doi.org/10.1175/1520-0469\(1980\)037<0630:TSATRT>2.0.CO;2](http://dx.doi.org/10.1175/1520-0469(1980)037<0630:TSATRT>2.0.CO;2), 1980.
- Moran, K. P., Martner, B. E., Post, M. J., Kropfli, R. A., Welsh, D. C., and Widener, K. B.: An Unattended Cloud-Profiling Radar for Use in Climate Research, *Bull. Amer. Meteor. Soc.*, 79, 443–455, doi:10.1175/1520-0477(1998)079<0443:AUCPRF>2.0.CO;2, [http://dx.doi.org/10.1175/1520-0477\(1998\)079<0443:AUCPRF>2.0.CO;2](http://dx.doi.org/10.1175/1520-0477(1998)079<0443:AUCPRF>2.0.CO;2), 1998.
- 10 Nakajima, T. and King, M. D.: Determination of the Optical Thickness and Effective Particle Radius of Clouds from Reflected Solar Radiation Measurements. Part I: Theory, *Journal of the Atmospheric Sciences*, 47, 1878–1893, doi:10.1175/1520-0469(1990)047<1878:DOTOTA>2.0.CO;2, [http://dx.doi.org/10.1175/1520-0469\(1990\)047<1878:DOTOTA>2.0.CO;2](http://dx.doi.org/10.1175/1520-0469(1990)047<1878:DOTOTA>2.0.CO;2), 1990.
- Platt, C. M. R.: Lidar and Radiometric Observations of Cirrus Clouds, *J. Atmos. Sci.*, 30, 1191–1204, doi:10.1175/1520-0469(1973)030<1191:LAROOC>2.0.CO;2, [http://dx.doi.org/10.1175/1520-0469\(1973\)030<1191:LAROOC>2.0.CO;2](http://dx.doi.org/10.1175/1520-0469(1973)030<1191:LAROOC>2.0.CO;2), 1973.
- 15 Rodgers, C. D.: *Inverse methods for atmospheric sounding : theory and practice*, World Scientific, Singapore; [River Edge, N.J.], <http://public.eblib.com/choice/publicfullrecord.aspx?p=1223583>, 2000.
- Rowe, P. M., Miloshevich, L. M., Turner, D. D., and Walden, V. P.: Dry Bias in Vaisala RS90 Radiosonde Humidity Profiles over Antarctica, *Journal of Atmospheric and Oceanic Technology*, 25, 1529–1541, doi:10.1175/2008JTECHA1009.1, <http://dx.doi.org/10.1175/2008JTECHA1009.1>, 2008.
- 20 Royer, A., Cliche, P., Marchand, N., Roy, A., Blanchard, Y., O'Neill, N. T., Damiri, B., Leclercq, J., Meunier, S., and Crozel, D.: An Automatic Sky Spectral Thermal Infrared Radiometer (ASSTIR) system, in: 4th Int. Symposium on Recent Advances in Quantitative Remote Sensing: RAQRS'IV, 22–26th September 2014, Torrent (Valencia), Spain., 2014.
- Sassen, K., Wang, Z., and Liu, D.: Global distribution of cirrus clouds from CloudSat/Cloud-Aerosol Lidar and Infrared Pathfinder Satellite Observations (CALIPSO) measurements, *Journal of Geophysical Research: Atmospheres*, 113, n/a–n/a, doi:10.1029/2008JD009972, <http://dx.doi.org/10.1029/2008JD009972>, d00A12, 2008.
- 25 Shupe, M. D.: A ground-based multisensor cloud phase classifier, *Geophys. Res. Lett.*, 34, L22 809–, <http://dx.doi.org/10.1029/2007GL031008>, 2007.
- Shupe, M. D., Walden, V. P., Eloranta, E., Uttal, T., Campbell, J. R., Starkweather, S. M., and Shiobara, M.: Clouds at Arctic Atmospheric Observatories. Part I: Occurrence and Macrophysical Properties, *Journal of Applied Meteorology and Climatology*, 50, 626–644, doi:10.1175/2010JAMC2467.1, <http://dx.doi.org/10.1175/2010JAMC2467.1>, 2011.
- 30 Shupe, M. D., Turner, D. D., Zwink, A., Thieman, M. M., Mlawer, E. J., and Shippert, T.: Deriving Arctic Cloud Microphysics at Barrow, Alaska: Algorithms, Results, and Radiative Closure, *Journal of Applied Meteorology and Climatology*, 54, 1675–1689, doi:10.1175/JAMC-D-15-0054.1, <http://dx.doi.org/10.1175/JAMC-D-15-0054.1>, 2015.
- Smith, W. L., Ma, X. L., Ackerman, S. A., Revercomb, H. E., and Knuteson, R. O.: Remote Sensing Cloud Properties from High Spectral Resolution Infrared Observations, *J. Atmos. Sci.*, 50, 1708–1720, doi:10.1175/1520-0469(1993)050<1708:RSCPFH>2.0.CO;2, [http://dx.doi.org/10.1175/1520-0469\(1993\)050<1708:RSCPFH>2.0.CO;2](http://dx.doi.org/10.1175/1520-0469(1993)050<1708:RSCPFH>2.0.CO;2), 1993.

- Sourdeval, O., Labonnote, L. C., Brogniez, G., Jourdan, O., Pelon, J., and Garnier, A.: A variational approach for retrieving ice cloud properties from infrared measurements: application in the context of two IIR validation campaigns, *Atmospheric Chemistry and Physics*, 13, 8229–8244, doi:10.5194/acp-13-8229-2013, <http://www.atmos-chem-phys.net/13/8229/2013/>, 2013.
- Stephens, G. L.: Cloud Feedbacks in the Climate System: A Critical Review, *Journal of Climate*, 18, 237–273, doi:10.1175/JCLI-3243.1, <http://dx.doi.org/10.1175/JCLI-3243.1>, 2005.
- Stephens, G. L. and Webster, P. J.: Clouds and Climate: Sensitivity of Simple Systems, *J. Atmos. Sci.*, 38, 235–247, doi:10.1175/1520-0469(1981)038<0235:CACSOS>2.0.CO;2, [http://dx.doi.org/10.1175/1520-0469\(1981\)038<0235:CACSOS>2.0.CO;2](http://dx.doi.org/10.1175/1520-0469(1981)038<0235:CACSOS>2.0.CO;2), 1981.
- Stephens, G. L., Tsay, S.-C., Stackhouse, P. W., and Flatau, P. J.: The Relevance of the Microphysical and Radiative Properties of Cirrus Clouds to Climate and Climatic Feedback, *J. Atmos. Sci.*, 47, 1742–1754, doi:10.1175/1520-0469(1990)047<1742:TROTMA>2.0.CO;2, <http://journals.ametsoc.org/doi/abs/10.1175/1520-0469%281990%29047%3C1742%3ATROTMA%3E2.0.CO%3B2>, 1990.
- Turner, D. D.: Microphysical properties of single and mixed-phase Arctic clouds derived from ground-based AERI observations, Ph.d. dissertation, University of Wisconsin - Madison, Madison, Wisconsin, <http://www.ssec.wisc.edu/library/turnerdissertation.pdf>, 2003.
- Turner, D. D.: Arctic Mixed-Phase Cloud Properties from AERI Lidar Observations: Algorithm and Results from SHEBA, *J. Appl. Meteor.*, 44, 427–444, doi:10.1175/JAM2208.1, <http://dx.doi.org/10.1175/JAM2208.1>, 2005.
- 15 Turner, D. D. and Eloranta, E.: Validating Mixed-Phase Cloud Optical Depth Retrieved From Infrared Observations With High Spectral Resolution Lidar, *Geoscience and Remote Sensing Letters*, IEEE, 5, 285–288, doi:10.1109/LGRS.2008.915940, 2008.
- Turner, D. D. and Löhnert, U.: Information Content and Uncertainties in Thermodynamic Profiles and Liquid Cloud Properties Retrieved from the Ground-Based Atmospheric Emitted Radiance Interferometer (AERI), *Journal of Applied Meteorology and Climatology*, 53, 752–771, doi:10.1175/JAMC-D-13-0126.1, <http://dx.doi.org/10.1175/JAMC-D-13-0126.1>, 2014.
- 20 Turner, D. D., Ackerman, S. A., Baum, B. A., Revercomb, H. E., and Yang, P.: Cloud Phase Determination Using Ground-Based AERI Observations at SHEBA, *J. Appl. Meteor.*, 42, 701–715, doi:10.1175/1520-0450(2003)042<0701:CPDUGA>2.0.CO;2, [http://dx.doi.org/10.1175/1520-0450\(2003\)042<0701:CPDUGA>2.0.CO;2](http://dx.doi.org/10.1175/1520-0450(2003)042<0701:CPDUGA>2.0.CO;2), 2003.
- Turner, D. D., Knuteson, R. O., Revercomb, H. E., Lo, C., and Dedecker, R. G.: Noise Reduction of Atmospheric Emitted Radiance Interferometer (AERI) Observations Using Principal Component Analysis, *J. Atmos. Oceanic Technol.*, 23, 1223–1238, doi:10.1175/JTECH1906.1, <http://dx.doi.org/10.1175/JTECH1906.1>, 2006.
- 25 Waliser, D. E., Li, J.-L. F., Woods, C. P., Austin, R. T., Bacmeister, J., Chern, J., Del Genio, A., Jiang, J. H., Kuang, Z., Meng, H., Minnis, P., Platnick, S., Rossow, W. B., Stephens, G. L., Sun-Mack, S., Tao, W.-K., Tompkins, A. M., Vane, D. G., Walker, C., and Wu, D.: Cloud ice: A climate model challenge with signs and expectations of progress, *Journal of Geophysical Research: Atmospheres*, 114, n/a–n/a, doi:10.1029/2008JD010015, <http://dx.doi.org/10.1029/2008JD010015>, 2009.
- 30 Wang, X. and Key, J. R.: Recent Trends in Arctic Surface, Cloud, and Radiation Properties from Space, *Science*, 299, 1725–1728, <http://www.sciencemag.org/content/299/5613/1725.abstract>, 2003.
- Warren, S. G. and Brandt, R. E.: Optical constants of ice from the ultraviolet to the microwave: A revised compilation, *J. Geophys. Res.*, 113, D14 220–, <http://dx.doi.org/10.1029/2007JD009744>, 2008.
- Wendisch, M., Yang, P., and Pilewskie, P.: Effects of ice crystal habit on thermal infrared radiative properties and forcing of cirrus, *Journal of Geophysical Research: Atmospheres*, 112, n/a–n/a, doi:10.1029/2006JD007899, <http://dx.doi.org/10.1029/2006JD007899>, 2007.
- 35 Winker, D. M., Pelon, J., Jr., J. A. C., Ackerman, S. A., Charlson, R. J., Colarco, P. R., Flamant, P., Fu, Q., Hoff, R. M., Kittaka, C., Kubar, T. L., Treut, H. L., McCormick, M. P., Mégie, G., Poole, L., Powell, K., Trepte, C., Vaughan, M. A., and Wielicki, B. A.:

- The CALIPSO Mission: A Global 3D View of Aerosols and Clouds, *Bulletin of the American Meteorological Society*, 91, 1211–1229, doi:10.1175/2010BAMS3009.1, <http://dx.doi.org/10.1175/2010BAMS3009.1>, 2010.
- Wylie, D. P. and Menzel, W. P.: Eight Years of High Cloud Statistics Using HIRS, *J. Climate*, 12, 170–184, doi:10.1175/1520-0442(1999)012<0170:EYOHCS>2.0.CO;2, <http://journals.ametsoc.org/doi/abs/10.1175/1520-0442%281999%29012%3C0170%3AEYOHCS%3E2.0.CO%3B2>, 1999.
- 5 Yang, P., Mlynczak, M. G., Wei, H., Kratz, D. P., Baum, B. A., Hu, Y. X., Wiscombe, W. J., Heidinger, A., and Mishchenko, M. I.: Spectral signature of ice clouds in the far-infrared region: Single-scattering calculations and radiative sensitivity study, *Journal of Geophysical Research: Atmospheres*, 108, doi:10.1029/2002JD003291, <http://dx.doi.org/10.1029/2002JD003291>, 4569, 2003.
- Yang, P., Tsay, S.-C., Wei, H., Guo, G., and Ji, Q.: Remote sensing of cirrus optical and microphysical properties from ground-based infrared radiometric Measurements-part I: a new retrieval method based on microwindow spectral signature, *IEEE Geoscience and Remote Sensing Letters*, 2, 128–131, doi:10.1109/LGRS.2005.844733, 2005.
- 10 Yang, P., Bi, L., Baum, B. A., Liou, K.-N., Kattawar, G. W., Mishchenko, M. I., and Cole, B.: Spectrally Consistent Scattering, Absorption, and Polarization Properties of Atmospheric Ice Crystals at Wavelengths from 0.2 to 100 μm , *Journal of the Atmospheric Sciences*, 70, 330–347, doi:10.1175/JAS-D-12-039.1, <http://dx.doi.org/10.1175/JAS-D-12-039.1>, 2013.